Original Paper

Landslides
DOI 10.1007/s10346-024-02365-y
Received: 28 June 2024
Accepted: 23 August 2024

Emilce Bustos · Gianluca Norini · Walter Ariel Báez · Pablo Grosse · Marcelo Arnosio · Lucia Capra

A new remote-sensing-based volcanic debris avalanche database of Northwest Argentina (Central Andes)

Abstract Volcanic debris avalanches are significant landslide events that shape volcanic landscapes globally. This study focuses on creating a comprehensive database of volcanic debris avalanches in Northwest Argentina through remote sensing analysis, leveraging the region's well-preserved deposits in arid conditions. The database includes morphometric parameters extracted from 12-m spatial resolution TanDEM-X digital elevation models and literature, providing insights into the occurrence and characteristics of these potentially catastrophic events. The methodology involved compiling bibliographic and cartographic data, manual digitization of collapse scars and deposits, and computation of morphometric parameters in a GIS, integrating structural lineaments and hydrothermal alteration zones. The database, which comprises 19 records, features detailed data on scars and deposits, morphometric characteristics, and additional layers for regional lineaments and hydrothermal alteration zones. Statistical analyses reveal correlations between various morphometric parameters, with most avalanche directions aligning perpendicularly to regional tectonic trends and hydrothermal alteration zones identified as significant factors in volcanic instability. The majority of collapses originate from composite volcanoes, with larger collapses linked to dacitic compositions. Collapses have ages between the Upper Miocene and Pliocene. We deem that the database, accessible via the IBIGEO website, will be a valuable tool for researchers and national authorities for geological risk assessment, enhancing the understanding of the spatial and temporal distribution of volcanic debris avalanches in the Central Volcanic Zone of the Andes. Continuous updates and fieldwork are essential to validate and expand the database, addressing gaps and confirming remote observations, thereby contributing to global knowledge on volcanic sector collapses and associated risks.

Keywords Volcano collapse · Morphometry · Scar · Volcanic debris avalanche deposit

Introduction

Volcanic debris avalanches are common landslide phenomena punctuating the evolution of many volcanic edifices worldwide (e.g., Roverato et al. 2021; Dufresne et al. 2021a, b). Volcanoes undergo cycles of construction and destruction throughout their lifespans, often involving large-scale gravitational collapses (Thouret 1999; Zernack and Procter 2021). They are susceptible to sector or flank collapses due to both exogenous and endogenous processes (McGuire 1996). For example, landslides can trigger violent explosive activity (e.g., Mount St. Helens; Voight et al. 1981) and generate tsunamis (e.g., Anak Krakatau; Williams et al. 2019). This susceptibility may persist after volcanic eruptive activity has ceased, making inactive volcanoes potentially dangerous. Thus, the hazard of sector collapses is often underestimated, despite posing a significant volcanic risk and being directly or indirectly responsible for injuries, fatalities, and economic loss (e.g., Auker et al. 2013; Williams et al. 2019).

The scientific and social importance of volcanic debris avalanches warrants the construction of databases on their occurrence and characteristics, allowing for the effective extraction and analysis of information from vast volumes of data (e.g., Giles 1995; Elmasri and Navathe 2011). Presently, there are numerous inventories of landslide events in volcanic environments, such as those of Japan (Ui et al. 1986; Inokuchi 2006), Indonesia (MacLeod 1989), New Zealand (Palmer et al. 1991; Neall 2002), Mexico (Capra et al. 2002), volcanic islands (Blahut et al. 2019), and other globally oriented databases (Dufresne et al. 2008, 2021b; Siebert and Roverato 2021). For the Central Andes, Francis and Wells (1988) used Landsat TM images to identify 28 volcanoes with collapse structures and 14 volcanic debris avalanche deposits. Since this publication, significant advancements have been made in the study of volcanic debris avalanches in the Central Andes, as evidenced by numerous scientific publications (e.g., Richards and Villeneuve 2001; van Wyk de Vries et al. 2001; Clavero et al. 2002; Wooller et al. 2004; Shea and van Wyk de Vries 2008; Davies et al. 2010; Godoy et al. 2012, 2017; Jicha et al. 2015; Rodríguez et al. 2020; Norini et al. 2020; Bustos et al. 2022).

The number of identified collapses in long-lived composite volcanoes depends on the preservation and exposure of the scar(s) and the debris avalanche deposits (e.g., Zernack and Procter 2021). In the Central Andes (Fig. 1), stratovolcanoes are characterized by relatively thick and viscous andesitic-dacitic lava flows. Furthermore, the low denudation rates of the region, due to the arid climate, result in particularly steep-sided edifices that are highly susceptible to collapse (e.g., Francis and Wells 1988; Grosse et al. 2009; 2014). Additionally, the high density of volcanoes and the exceptional preservation of the deposits—thanks to the prevalent arid conditions and lack of vegetation—make this region favorable for remote sensing studies.

The aim of this publication is to present a new and comprehensive volcanic debris avalanches database for NW Argentina, which compiles morphometric parameters extracted from Digital Elevation Models (DEM) and information from existing scientific literature. The quantitative parameters that characterize both the scars and the volcanic debris avalanche deposits are then analyzed to provide new insights into the occurrence and characteristics of these potentially catastrophic events. The database

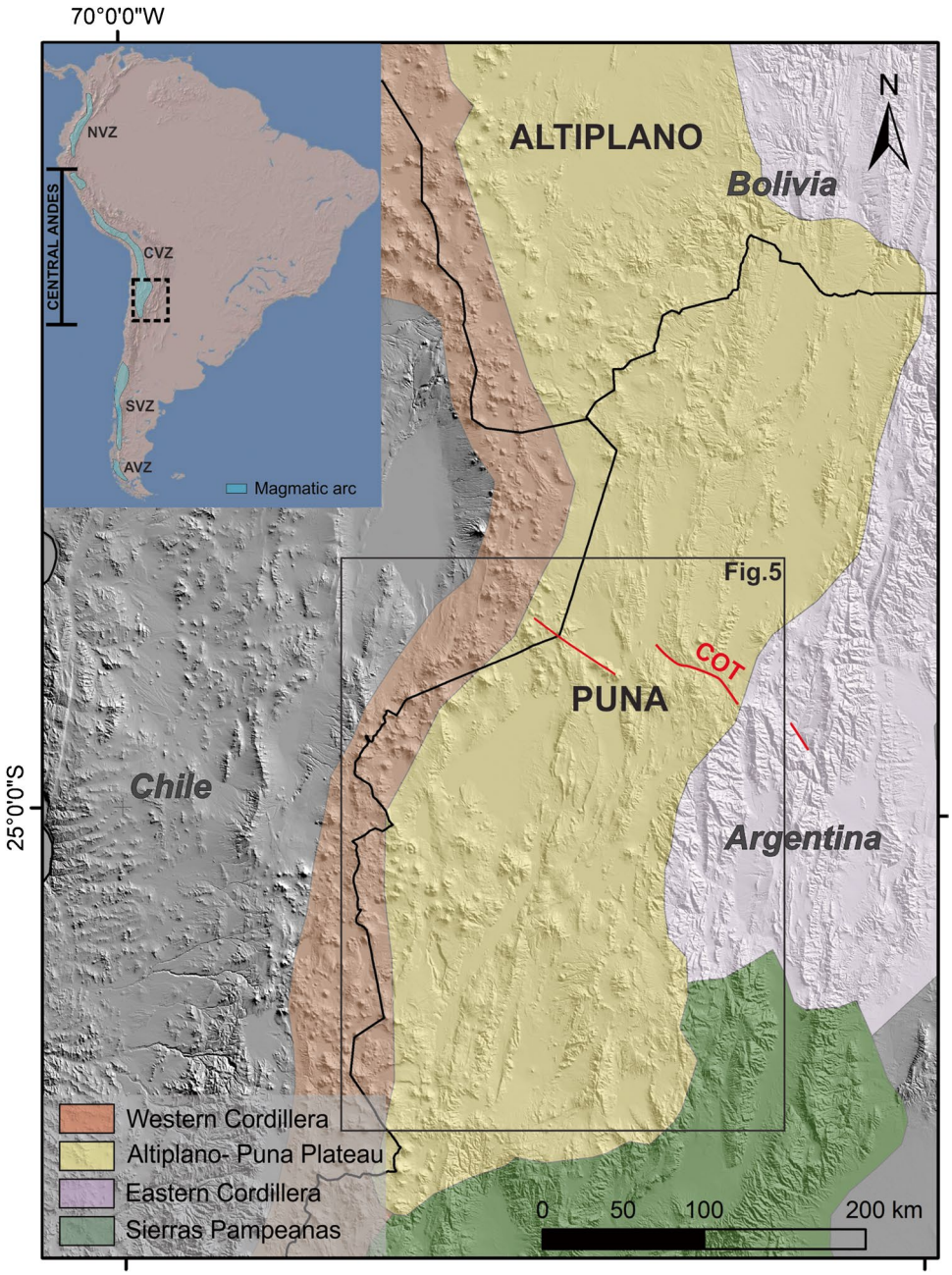

Fig. 1 Shaded relief SRTM DEM of the southern part of the Central Andes showing major geological provinces (after Grosse et al. 2017). COT Calama–Olacapato–El Toro lineament. The extension of Fig. 5 is shown (black rectangle). Inset in the upper left corner is a map of South America showing the four Andean volcanic zones and the Central Andes region. NVZ Northern Volcanic Zone, CVZ Central Volcanic Zone, SVZ Southern Volcanic Zone, AVZ Austral Volcanic Zone, based on Stern et al. (2007)

should constitute a valuable tool for understanding the spatial and temporal distributions of volcanic debris avalanches in the Central Volcanic Zone of the Andes and for increasing the knowledge about the geometries and mechanisms or factors associated with volcanic sector collapses worldwide.

Geological framework

The Central Andes extend across parts of Peru, Bolivia, Chile, and Argentina, spanning from 5 to 33° S (Fig. 1). This orogenic belt includes the Peruvian flat slab segment to the North, the Central Volcanic Zone (CVZ), and the Pampean flat slab to the South. The

volcanism is the result of the subduction of the Nazca plate under the South American Plate (e.g., James 1971). The CVZ includes active and potentially active volcanoes located between approximately 13 and 28° S, with volcanoes recognized since the Oligocene (e.g., Parada et al. 2007).

In Northwest Argentina, volcanism is distributed within the Western Cordillera (arc) and extends into the back-arc region, encompassing the Puna area (Fig. 1). The arc roughly coincides with the international boundary between Argentina and Chile, while back-arc volcanism extends eastward mainly along NW–SE trending transverse volcanic chains (e.g., Viramonte et al. 1984; Riller et al. 2001; Acocella et al. 2011; Norini et al. 2013).

The Altiplano–Puna Plateau (in Bolivia and Argentina, respectively) is the world's second-highest and largest continental plateau after the Tibetan (Fig. 1). This elevated and relatively flat region is characterized by the most voluminous caldera-forming ignimbrites on Earth, stratovolcanoes, lava domes, and mafic monogenetic volcanism (e.g., de Silva 1989; Lindsay et al. 2001; Trumbull et al. 2006; Kay and Coira 2009; Báez et al. 2023). The main fault system within the Puna region is known as the Calama–Olacapato–El Toro Lineament (COT) (Fig. 1; e.g., Viramonte et al. 1984; Salfity 1985; Acocella et al. 2007; Norini et al. 2013). This geological feature represents a significant component of crustal deformation, stretching approximately 300 km in length and with a maximum width of approximately 10–20 km (Allmendinger et al. 1983; Acocella et al. 2007; Norini et al. 2013).

The abundance of large stratovolcanoes with steep slopes makes the Central Andes a zone with a high risk of gravitational flank and sector collapse (Francis and Wells 1988). Francis and Wells (1988) identified collapse structures in the Central Andes and found that, in general, cones with collapse structures and deposits develop perpendicular to the regional tectonic elements, suggesting that the collapses could be related to a seismic component. Despite the favorable conditions for the remote identification of avalanches, very few avalanches have been studied in detail in NW Argentina, namely Socompa (the avalanche deposit is emplaced on Chilean soil; Francis et al. 1985; Wadge et al. 1995; van Wyk de Vries et al. 2001; Wooller et al. 2004; Kelfoun and Druitt 2005; Kelfoun et al. 2008; Davies et al. 2010; Grosse et al. 2022), Llullaillaco (two deposits, named north and east in our work; Richards and Villeneuve 2001; Shea and van Wyk de Vries 2008), Lastarria (Naranjo and Francis 1987; Rodriguez et al. 2020), and Chimpa (Norini et al. 2020; Bustos et al. 2020, 2022).

Database design and architecture

The design of the database architecture is premised on ensuring that all the information contained is both comparable and consistent, allowing for effective data contrast and analysis. The complete volcanic debris avalanche database consists of a Microsoft Excel spreadsheet, and five point, line, and polygon vector files in kmz format (Supplementary material).

According to Bernard et al. (2021), a volcanic debris avalanche (VDA) is defined as a rapid, water-unsaturated, gravity-driven mass movement comprising, generally, multiple volcanic units. This phenomenon manifests in the field as a landslide scar on the volcanic edifice and a volcanic debris avalanche deposit at its foot. The scar is a concave depression in the volcano with steep walls, while the debris avalanche deposit is an epiclastic breccia, composed of pieces of the source edifice, materials incorporated along the transport path, and occasionally, elements from the volcano's basement or substratum.

Considering these definitions, the database comprises three main classes and GIS vectors, "volcano," "scar," and "volcanic debris avalanche deposit," all connected via the "volcano" field (Fig. 2). The data within each of these classes are recorded in distinct fields, each corresponding to specific columns in the database (Tables 1, 2, and 3).

Classes

Volcano class (volcano database section and volcano point kmz file)

This point layer aggregates data on all volcanic edifices in Northwest Argentina. It draws from various sources, including the Smithsonian Institute database (Global Volcanism Program, 2024), a database of composite volcanoes of NW Argentina (Grosse et al. 2017), and other scientific publications. For each volcano, the database contains fields storing information on the name, type of volcano (composite volcano, shield, dome, dome complex, mafic monogenetic, caldera, etc.), coordinates (latitude and longitude), geochemical composition, relative age, presence or absence of hydrothermal alteration, whether a collapse occurred (yes, no, uncertain), and the number of collapses (Table 1).

Scar class (scar database section and scar polyline kmz file)

This layer delineates with polylines the scars present on the volcanoes of the region. The first field contains the name of the volcano to which the structure is associated, along with the scar name and the name of the related volcanic avalanche debris deposit. The preservation degree (well-defined, defined, moderately defined, and poorly defined) and plan view shape (semicircular, U-shaped, horseshoe, triangular, irregular, rectilinear) are recorded. In addition, the quantitative parameters that characterize the scar (following Bernard et al. 2021; Table 2) are provided for the scars related to an identified debris avalanche deposit. An observation field is included to specify reasons certain morphometric parameters were not calculated and a field with the possible trigger for the collapse. The final field pertains to the bibliography.

Volcanic debris avalanche deposit class (VDAD database section and VDAD polygon kmz file)

This polygon vector layer maps the extent of the volcanic debris avalanche deposits. The first column specifies the name of the volcano associated with the deposit, while the second column records the name of the deposit (if no name has been previously assigned, the volcano's name is used), and the third, the deposit association to collapse. Plan view shape and age of the deposit are recorded. Quantitative parameters of the VDAD, such as length, width, area, height, slope, thickness, volume, runout length, drop height, and apparent friction coefficient, are logged (Table 3). When available, parameters sourced from literature are incorporated into the database and denoted in the kmz file with a "b" (e.g., deposit length from bibliography, LD_b). Parameters derived from GIS analyses are indicated with an "m" in the kmz

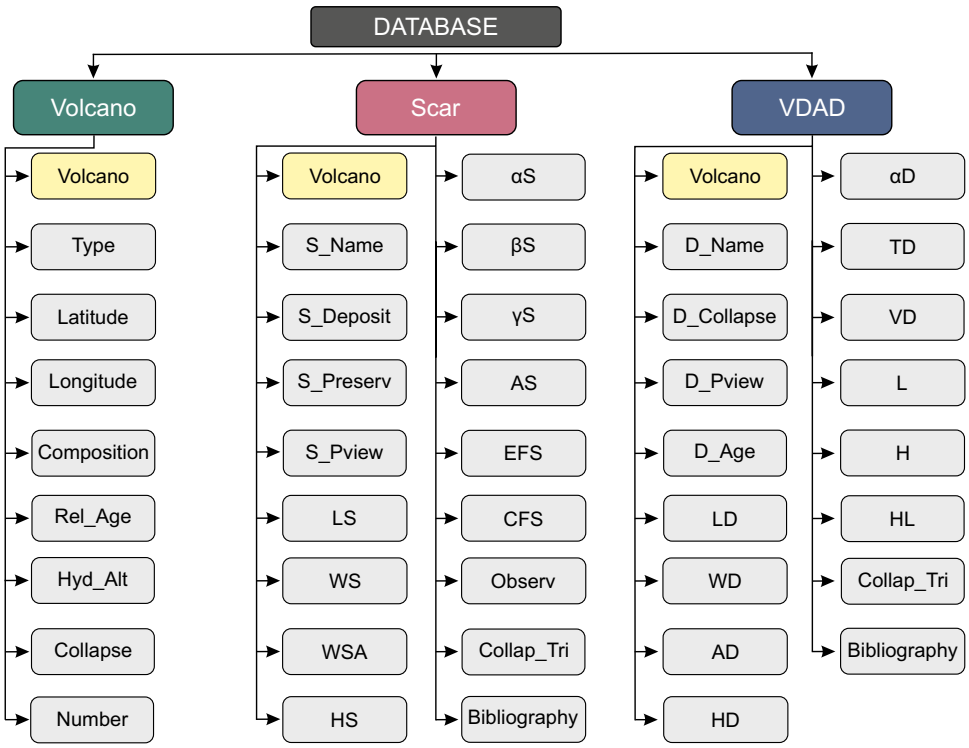

Fig. 2 Diagram showing the fields in each database class. In yellow are highlighted common fields in the three classes. Field name abbreviations are used. The complete field names are given in Tables 1, 2, and 3

Table 1 List of the parameters used in the "volcano" database section and kmz file

Field name abbreviation	Field name	Field description
Volcano	Volcano	Volcano name
Type	Type	Composite volcano, shield, dome, dome complex, caldera, mafic monogenetic
Latitude	Latitude	
Longitude	Longitude	
Compositio	Composition	Main composition
Rel_Age	Relative age	Relative age of the volcanism
Hyd_Alt	Hydrothermal alteration	Presence or absence of hydrothermal alteration (yes, no)
Collap	Collapse	Yes, no, uncertain
Number	Number of collapses	Numerical field

file (e.g., deposit length from our own measurements: LD_m). The last fields store the potential triggers for the collapse and the bibliography related to the VDAD.

Regional tectonic structures and zones of hydrothermal alteration are factors that can contribute to volcanic instability (e.g., Lagmay et al. 2000; Reid et al. 2001; Roverato et al. 2021; Bustos et al. 2022). In this sense, and as a complement to the database, the following data layers were created:

i. Regional lineaments: a polyline vector file where regional structural features are recorded.
ii. Hydrothermal alteration zones: the occurrence of hydrothermal alteration affecting the volcanoes is registered in a point-type vector layer.

Table 2 List of the parameters listed in the "scar" database section and kmz file

Field name abbreviation	Field name	Field description
Volcano	Volcano	Name of the volcano that hosts the scar
S_Name	Scar name	Scar name; if there is no name in the bibliography, the name of the volcano that hosts the scar is assigned
S_Deposit	Scar deposit	Volcanic debris avalanche deposit name associated with the scar *VDAD* is *unknown* when the scar is associated with a possible collapse event not identified in the bibliography
S_Preservation	Scar preservation	Degree of preservation of the scar *Well-defined*, *defined*, *moderately defined*, *and poorly defined* *No visible scar* when the scar cannot be recognized
S_Pview	Scar plan view	Shape of the scar in plan view *Semicircular*, *U-shaped*, *horseshoe*, *triangular*, *irregular*, *rectilinear*
LS	Scar length	Distance from the headwall to the middle of the aperture
WS	Scar width	Maximum distance between the sidewalls, orthogonal to the length
WSA	Scar aperture width	Distance between the sidewalls at the aperture
HS*	Scar height	Height between the top of the headwall and the aperture
αS (AlphaS)	Scar aperture angle	Angle between the lines drawn from the headwall to the sidewalls extremity
βS* (BetaS)	Scar slope	Slope between the top of the headwall and the aperture; βS = atan HS/LS
γS (GammaS)	Scar azimuth	Azimuth of scar length
AS	Scar area	Surface of the scar in the plan view
EFS	Elongation factor	Ratio between the scar length and width; EFS = LS/WS
CFS	Closure factor	Ratio between the scar aperture width and the scar width; CFS = WSA/WS
Observ	Observations	Clarification of reasons why some parameters were not measured.
Collap_Tri	Collapse trigger	Event trigger, if known
Bibliograp	Bibliography	References

*This data is derived from the reconstruction of the pre-collapse topography. As such, it is only available in publications that have undertaken this reconstruction or when the defining characteristics made the reconstruction straightforward and minimally speculative

Methods

The methodology included a first stage of bibliographic and cartographic recompilation and volcanic scar and debris avalanche deposit identification, a second step of manual digitalization of scars and volcanic debris avalanche deposits, and a third stage of computation of their morphometric parameters in a GIS. A fourth phase consisted of the digitalization of two additional layers regarding structural lineaments and hydrothermal alteration.

Identification of scars and volcanic debris avalanche deposits

First, using previously published databases, volcanoes present in the region were located, and data regarding their typology, composition, and relative age were obtained (e.g., Global Volcanism Program 2024; Grosse et al. 2017). It is worth noting that for volcanoes without names, their latitude value was assigned as their name following the methodology of Grosse et al. (2017).

Table 3 List of the parameters used in the "volcanic debris avalanche deposit" database section and kmz file

Field name abbreviation	Field name	Field description
Volcano	Volcano	Name of the volcano related to the volcanic debris avalanche deposit
D_Name	Deposit name	Volcanic debris avalanche deposit name; if there is no name in the bibliography, the name of the volcano related to the deposit is assigned
D_Collapse	Collapse-associated deposit	Indication if the deposit is recognized in the bibliography as a volcanic landslide or if it is unknown (suspected of constituting a deposit due to its morphological characteristics) *VDAD, VDAD unknown*
D_PView	Deposit plan view	Deposit morphology in plan view *fan-shaped, wedged, bifurcated, elongated, lobed, fingered, circular*
D_Age	Deposit age	Age of the event, if known
LD	Deposit length	Distance between the front and the tail of the deposit
WD	Deposit width	Maximum distance between the deposit margins, orthogonal to the length
AD	Deposit area	Surface covered by the deposit in the plan view
HD	Deposit height	Altitude difference between the tail and the front of the deposit
αD (AlphaD)	Deposit declivity	Average slope between the tail and the front of the deposit (aD = atan HD/LD)
TD*	Deposit thickness	Average thickness of the deposit
VD*	Deposit volume	Volume of the deposit (VD = AD TD)
L	Runout length	Distance between the scar headwall and the deposit front
H	Drop height	Altitude difference between the maximum pre-landslide topography and the deposit front
HL	Apparent friction coefficient	Ratio between the drop height and runout length
Collap_Tri	Collapse trigger	Event trigger, if known
Bibliograp	Bibliography	References

*This data is derived from the reconstruction of the pre-collapse topography. As such, it is only available in publications that have undertaken this reconstruction or when the defining characteristics made the reconstruction straightforward and minimally speculative

Subsequently, scars and volcanic debris avalanche deposits were identified. Previously identified and studied deposits in the literature were considered. Additionally, scars and deposits previously unrecognized or unstudied were identified through analysis using the Landsat ETM + satellite imagery and Tandem-X DEMs covering the entire region.

Digitalization of scars and volcanic debris avalanche deposits

The digitalization of scars and volcanic debris avalanche deposits relied on high-resolution satellite imagery (e.g., CNES Airbus, Global Eye images from Google Earth) and the TanDEM-X DEM with 12-m spatial resolution (Krieger et al. 2007). DEM derivatives, such as slope maps and shaded relief images, were used to enhance feature detection.

Landslides previously identified in the scientific literature were added to the database. Additionally, satellite imagery analysis (Landsat ETM + , high-resolution images from Google Earth) and DEMs were used to identify and confirm areas showing morphological characteristics of possible previously unreported volcanic landslides.

Calculation of morphometric parameters

The database includes the quantification of various morphometric parameters characterizing both the scar and the volcanic debris avalanche deposits (VDAD), following the definitions of Bernard et al. (2021) (Figs. 2 and 3; Tables 2 and 3). Measurements were calculated in GIS using the TanDEM-X DEMs. In some instances, the inherent characteristics of the scar preclude certain measurements. For example, Chimpa volcano has two linear-parallel scars (Fig. 4a); Tuzgle volcano shows an incomplete scar (Fig. 4b), and − 24.91 volcano lacks a visible scar (Fig. 4c). Calculations include the length, width, aperture width and angle, azimuth, and area of the scar

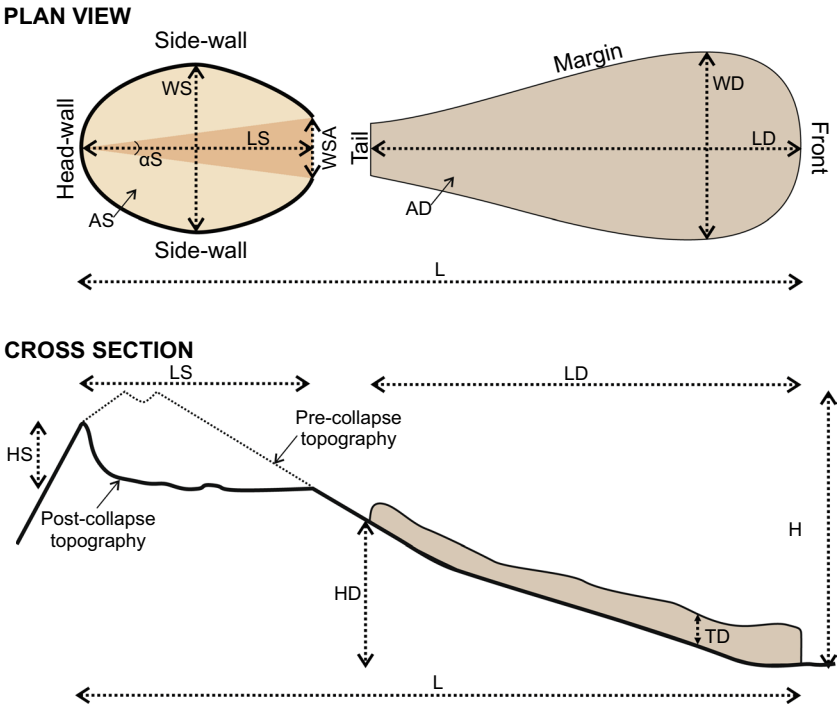

Fig. 3 Sketch showing the quantitative parameters for the scars and volcanic debris avalanche deposits. After Bernard et al. (2021). Abbreviations can be consulted in Tables 2 and 3

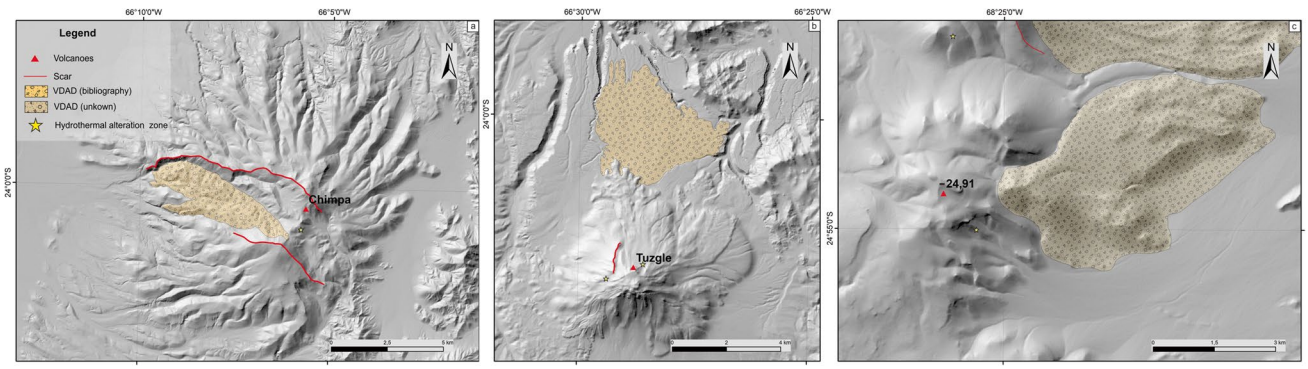

Fig. 4 Examples of volcanoes with issues in measuring parameters of the scar. **a** Chimpa volcano, **b** Tuzgle volcano, and **c** – 24.91

(Table 2; Fig. 3). The height, together with ratios among various parameters such as slope, elongation factor, and closure factor, was also computed (Table 2). Regarding VDAD, measurements incorporate length, width, area, height, runout length, and drop height (Table 3; Fig. 3). Deposit thickness estimation, and consequently volume, usually requires field studies of the VDA deposit. Consequently, these parameters are only available when they are calculated in the bibliography.

Digitalization of additional layers

A polyline vector file of regional structural features was also created following the existing bibliography and geological maps (Blasco et al. 1996; Zappettini et al. 2001; Hongn et al. 2001; Coira et al. 2004; Seggiaro et al. 2006, 2007, 2015), and through the analysis of shaded relief images derived from the TanDEM-X DEMs, which highlight these structures.

The occurrence of hydrothermal alteration on volcanoes was mapped in a point-type vector layer. Hydrothermally altered areas were identified through multispectral analysis of Landsat ETM + satellite data using the classical geological mapping combination RGB 742 (e.g., Turner et al. 2008; Laake 2011; Hasan et al. 2016), and a critical recompilation of literature data (e.g., Blasco et al. 1996; Zappettini et al. 2001; Hongn et al. 2001; Coira et al. 2004; Seggiaro et al. 2006, 2007, 2015).

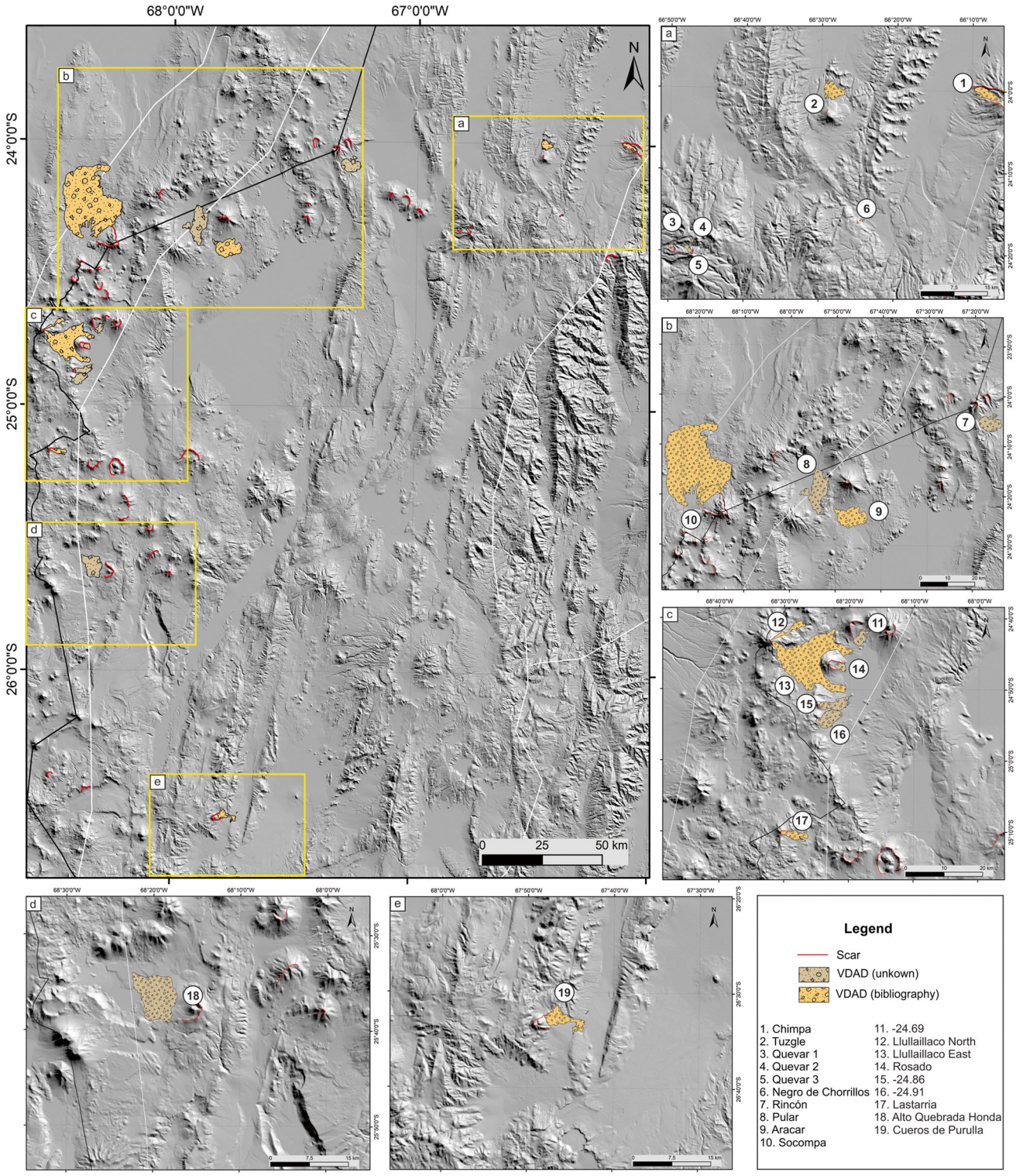

Fig. 5 Distribution of scars and volcanic debris avalanche deposits in NW Argentina. White polylines are boundaries between geological provinces (Fig. 1). Background image is SRTM DEM-derived shaded relief

Results: database analysis

Volcanic debris avalanche distribution and frequency

The database of volcanic debris avalanches comprises a total of 19 records from across NW Argentina (Fig. 5). Of these, 15 are complete (including both scar and VDAD), whereas four only contain the landslide deposit information because morphometric parameters of the scars could not be determined (Chimpa, Tuzgle, East Llullaillaco, and – 24.91 volcanoes). Five of the 19 entries have been previously studied in detail, five have been documented in regional maps or studies, and nine are recognized in this study (Fig. 5).

No evidence of avalanches was found in the northern portion of the Puna. In the central area, volcanic debris avalanche deposits from five volcanoes are located along or near the NW–SE trending COT lineament (Tuzgle, Chimpa, Rincón, Quevar, Negro de Chorrillos). Moving southward, avalanche deposits concentrate along the main N-S trending volcanic arc (Western Cordillera; Aracar, Pular, Socompa, Llullaillaco, – 24.86, Cerro Rosado, – 24.69, – 24.91, Lastarria, Quebrada Honda). Further south, at the southernmost tip of the Puna, only one event is recorded in the back-arc region (Cueros de Purulla). Most deposits entered in the database are associated with stratovolcanoes, with only two exceptions, the Negro de Chorillos monogenetic scoria cone and the Cueros de Purulla rhyolitic dome complex. The most significant collapse events are associated with composite volcanoes of dacitic composition (six volcanoes, including Socompa and Llullaillaco), but there are also collapse events recorded in andesitic-dacitic (five volcanoes) and andesitic (six volcanoes) centers.

The scarcity of radiometric dates for collapse events makes it difficult to assess their frequency. Only three avalanches have radiometric constraints. The Llullaillaco collapse occurred at or after 150 ka (Pleistocene; Richards and Villeneuve 2001), the Lastarria avalanche deposit has been dated at 7430 + 136–156 cal. year B.P. (Holocene; Rodríguez et al. 2020), and the Socompa event has been constrained to 6.18 ka + 0.28–0.64 (Holocene; Grosse et al. 2022). Relative ages of volcanism allow for establishing possible ages of the volcanic debris avalanche formation. In the area, several events could have occurred in the Upper Miocene (e.g., Chimpa, Rincón, Alto Quebrada Honda) and the Pliocene–Lower Pleistocene (Aracar). The most recent records of volcanic debris avalanches are probably related to Pleistocene (Pular, Negro de Chorrillos, Cueros de Purulla) and Upper Pleistocene–Holocene (Tuzgle) volcanism. However, these assessments constitute only an approximation since, especially for the older volcanoes, the collapse process may have occurred long after the last effusive or explosive activity of the volcano (e.g., Roverato et al. 2021).

Morphological and morphometric features of scars and debris avalanche deposits

In plan view, the most common scar morphology is semi-circular, with the width approximately twice its length (nine cases, e.g., Llullaillaco, Alto Quebrada Honda; Fig. 5). Divergent linear sidewalls, i.e., triangular scars, are recorded at three volcanoes (Socompa, Lastarria, and Cueros de Purulla). Rectilinear scars are found at Chimpa and Tuzgle volcanoes, while U-shaped scars (with a semicircular headwall and parallel sidewalls, where the length is greater than the width) characterize Rincón and Cerro Rosado scars. One irregular scar is registered at the Aracar volcano. Horseshoe scars (with an aperture width smaller than their maximum width) are not reported in this database. In plan view, the most common configurations for the volcanic debris avalanche deposit are elongated (mainly confined by valley walls; six cases, e.g., Lastarria, Chimpa) and irregular (seven cases, e.g., Aracar, Quevar 1, Alto Quebrada Honda). Fan-shaped morphologies (unconfined deposits with a large concave front) are found at Rincón, Tuzgle, Socompa, and Cueros de Purulla. Finally, a circular plan view morphology is recorded at – 24.91 volcano.

The basic morphometric characteristics of the scars and volcanic debris avalanche deposits are summarized in a series of box-and-whisker plots (Figs. 6 and 7). The morphometric parameters characterizing the scars have great variability (Fig. 6). The Socompa scar is by far the largest, with outlier values for length (7.54 km), width (8.65 km), and aperture width (9.26 km) (Fig. 6). On the other hand, the Quevar 3 scar has the smallest length (133 m) and the Negro de Chorrillos scar has the smallest width (319 m). The median scar length is ~1 km, with most values falling between ~100 m and 3 km (Fig. 6). The median scar width is ~2 km, with the highest frequency of data ranging between ~300 m and 3 km. The median scar aperture width is ~2 km, while most of the data is distributed between ~350 m and ~4 km. Most scar height values fall between ~100 and 900 m, with a median of 580 m. The median of the aperture angle is 80°, and the median azimuth is 115° (southeast) (Fig. 6).

There are also significant variations in the morphometric values for volcanic debris avalanche deposits (Fig. 7). The length of the deposits has symmetric values with a median of ~7 km, with most of the data ranging between ~3 and 9 km. Outliers in length include Socompa (~39 km) and Llullaillaco East Avalanche (23 km), both corresponding to globally significant large-scale collapse events. Regarding width, the data is mainly concentrated between ~2 and 8.5 km, with a median of 3.6 km. The deposit height has a median of ~500 m, with one outlier at 2.8 km corresponding to the Llullaillaco east avalanche. Finally, the deposit declivity has a median of 0.11°, with the majority of the data falling between 0.04 ando.17°.

Basic relations between the morphometric characteristics of the scars have been expressed by fitting a linear regression statistical model (e.g., Dufresne et al. 2021b). The same model was used to characterize the apparent friction coefficient (e.g., Devoli et al. 2009; Blahut et al. 2019; Dufresne et al. 2021b). The relationship between the area and the runout length has been articulated through the application of a power model (e.g., Dufresne et al. 2021b). The accuracy of the fitting is characterized by employing the adjusted coefficient of determination (R^2). Scatter plots were used to analyze pairs of morphometric parameters of the scars and deposits (Fig. 8). The strongest correlation is observed in the closure factor, showing a positive trend. A similar linear positive trend is recorded for the elongation factor, although the R^2 value is slightly lower. A low logarithmic correlation is observed for the apparent friction coefficient; for example, for runout length values around 9 km, the corresponding drop height values range from 700 to 1500 m. The area and runout length are strongly and positively related through a power function.

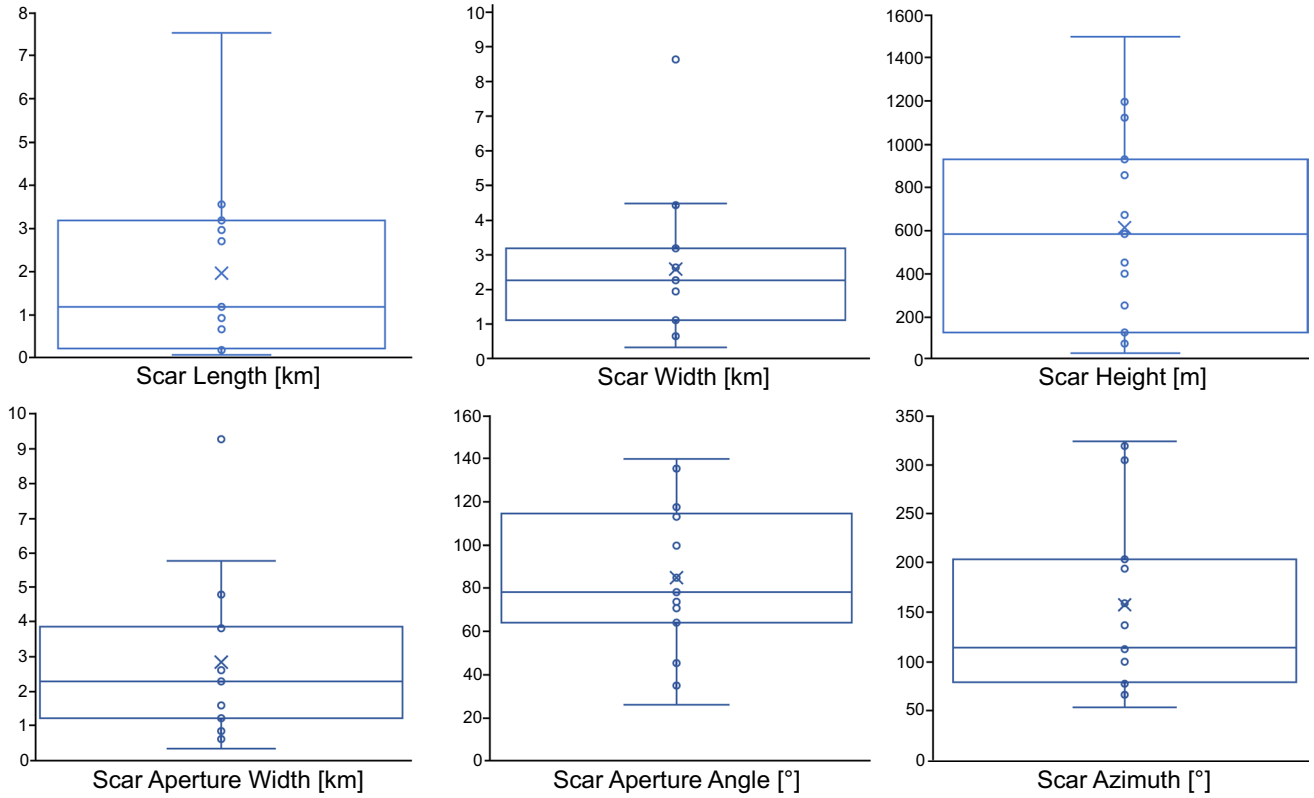

Fig. 6 Box-and-whisker plots showing the morphometric characteristics of the scars. The box shows the median along with the 1st and 3rd quartiles. The whiskers show the ± 1.5 * interquartile range

Correlations between volcanic debris avalanches, lineaments, and hydrothermal alteration

Through the analysis of regional geological maps and DEM-derived shaded relief images, the most significant lineaments in the studied area were mapped (Fig. 9). The length of these lineaments varies between 1 and 50 km. The primary trend of the lineaments is NNE–SSW (mean azimuth of N 005°; Fig. 10a).

Analyzing the database and considering the gamma angle, which represents the azimuth of the scar, most avalanche directions are perpendicular to the predominant regional lineament trend (Fig. 10b). There are some exceptions, such as the Tuzgle deposit extending to the north and the Rincón avalanche towards the SE (Fig. 10b).

As an annex to the database, areas with visible surface hydrothermal alteration were identified using satellite images to correlate volcanic edifice instability events with zones of hydrothermal alteration (Fig. 9). Out of the 19 documented collapse events in the database, ten are spatially associated with hydrothermal alteration zones. For instance, hydrothermal alteration is observed at the summits of the Cerro Rosado, − 24.69, − 24.91, and − 24.86 volcanoes, all of which are related to a volcanic debris avalanche deposit (Fig. 11). On the other hand, the peak of Llullaillaco shows no signs of hydrothermal alteration, although this could be due to the presence of younger products occupying the summit, which may have obliterated previous deposits that might have been altered.

Discussion

VDAD spatial and temporal distribution in the Central Andes context

On a global scale, 50% of recognized volcanic debris avalanche deposits are located in Japan, the American continent, and Russia (Dufresne et al. 2021b). The volcanic debris avalanche database of the Central Andes, compiled by Francis and Wells (1988), consists of 14 records located within the volcanic arc spanning Bolivia, Argentina, and Chile. Our contribution adds 15 records, complementing this database. The database analysis presented in this work enables the identification of the spatial distribution of volcanic debris avalanche deposits in NW Argentina. The volcanic debris avalanche deposits are concentrated along the NW–SE COT area and towards the south along the N–S axis of the volcanic arc (Western Cordillera) (Fig. 5). Volcanic avalanches were not detected in the northern zone of the Puna, which may be due to their absence or poor preservation. In this area, volcanoes are older and collapse calderas and associated ignimbrite deposits are more frequent, which may mask previous avalanches/landforms. The majority of identified debris avalanche deposits in NW Argentina are associated with composite volcanoes, similar to the globally calculated percentages (e.g., three-fourths of all known collapse events are from stratovolcanoes, Dufresne et al. 2021b). Two exceptions were recorded, corresponding to a scoria cone (Negro de Chorillos) and a dome complex (Cueros de

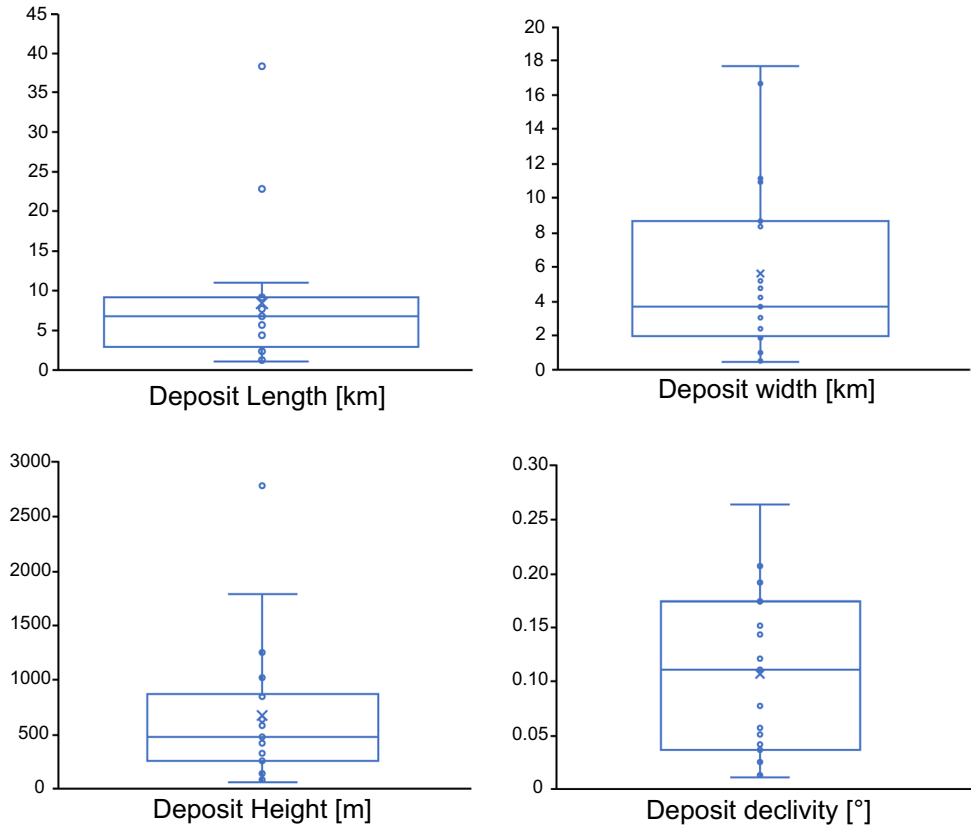

Fig. 7 Box-and-whisker plots showing the morphometric characteristics of the volcanic debris avalanche deposits. The box shows the median along with the 1st and 3rd quartiles. The whiskers show the ± 1.5 * interquartile range

Purulla). The larger collapse events documented in the database are linked to dacitic compositions.

On average, more than five collapse events per century have been reported worldwide since 1500 AD (Siebert and Roverato 2021). Globally, the question remains whether volcano collapses are more common in recent times or if, on the contrary, there is a bias due to the preservation of collapse features, as scars and avalanche deposits can be eroded, obliterated, or covered by more recent activity. The temporality of the volcanic debris avalanche phenomena in NW Argentina cannot be assessed due to the scarcity of data. Reported information indicates collapse events in the Pleistocene (Llullaillaco; Richards and Villeneuve 2001) and Holocene (Lastarria and Socompa; Rodríguez et al. 2020; Grosse et al. 2022). The relative ages of volcanism allow for an approximation of the collapse ages in the new records provided by our work. The oldest recorded collapses could have occurred in the Upper Miocene (e.g., Chimpa, Rincón), whereas others probably occurred in the Pliocene–Lower Pleistocene (e.g., Aracar), Pleistocene (e.g., Cueros de Purulla), and Upper Pleistocene–Holocene (e.g., Tuzgle). It is important to note that the eruptive history of composite volcanoes involves both construction and destruction events (e.g., Thouret 1999). This dynamic makes it difficult to recognize ancient collapse events using remote sensing techniques, especially in volcanic edifices that have continued with construction events, obliterating the features associated with volcanic debris avalanche events (e.g., Roverato et al. 2021). This impacts the recognition of the true recurrence of these phenomena throughout the lifespan of a volcanic edifice.

Comparison of morphometric parameters with Central Andes and global values

The database contains morphometric parameters for both the scar and the volcanic debris avalanche deposits. The morphometric parameters should be considered with caution, as a scar can undergo erosion or be filled with material over time, potentially leading to changes in its morphology (e.g., Siebert et al. 2004; Bernard et al. 2008, 2021). Dimensionless parameters such as closure factors and elongation are more robust for comparisons of scars of different sizes (Fig. 8; Bernard et al. 2021).

For the Central Andes, which includes records also found in our database, the average friction coefficient value is 0.1 and the median is 0.11 (Francis and Wells 1988). The values obtained for events recorded in Northwest Argentina are higher, with an average of 0.17 and a median of 0.15 (Fig. 12). In our database, we identified smaller-scale events that were previously unknown, with lower values of runout length and drop height (Fig. 12a), occupying a smaller area (Fig. 12b). A significant portion of the records have a runout length and drop height of less than 2 km (Fig. 12a). The apparent coefficient of friction, which describes the mobility of the volcanic debris avalanche, also shows the shorter distances reached by several records included in our database compared to the Central

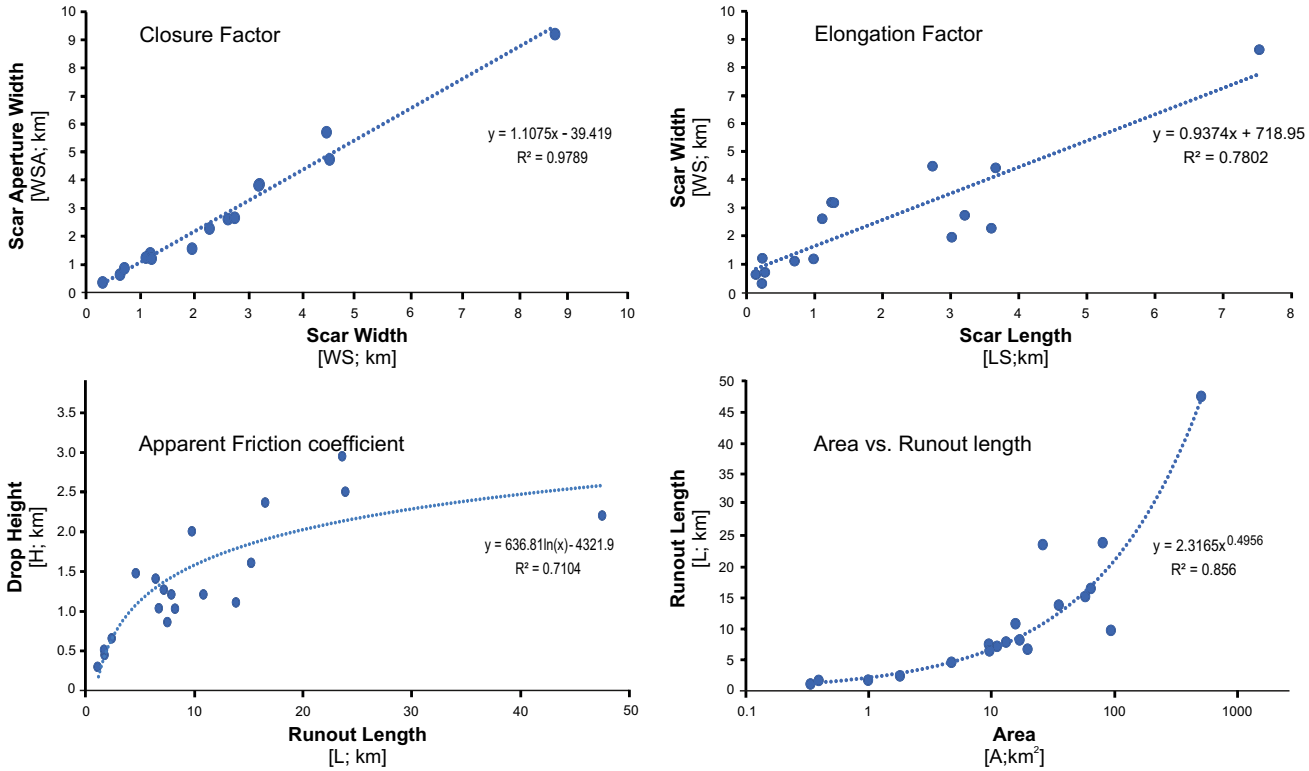

Fig. 8 Dispersion graphs showing the closure factor, elongation factor, apparent friction coefficient, and area vs runout length. Equation and *R*-value are shown

Andes database (Fig. 12b). Our approach, using a detailed DEM, allowed the determination of minor collapses. On the other hand, the logarithmic adjustment in the apparent friction coefficient plot (Fig. 8) indicates that above a drop height of approximately 1.5 km, the mobility of volcanic debris avalanches may depend on other factors besides the volume such as slope, topography, source material, path material, and water content (e.g., Aaron and McDougall 2019; Bernard et al. 2021).

The morphometric parameters obtained in our database are compared in Fig. 13 with the global avalanche compilation of Dufresne et al. (2021b). Avalanche volume was not considered, as the measurement of VDAD volume is, in most cases, highly speculative, with the area being more reliable (e.g., Bernard et al. 2021). Our data shows consonance with global records (Fig. 13). The comparison between runout length and area shows that our data trend is parallel to and slightly lower than the global data. In NW Argentina, volcanic debris avalanche records are somewhat shorter, although this difference is probably not significant. Our data reflects several minor events, although most of these parameters in our database are consistent with globally recorded data (Fig. 13a). On the other hand, the slope of the regression line in the drop height vs runout length plot is much steeper (Fig. 13b), meaning that for similar drop height values, the studied volcanic avalanches exhibit higher runout length values (Fig. 13b). Therefore, our database records lower friction coefficients, indicating greater mobility of these volcanic avalanches. It is also important to note that in this case, most of the data have values consistent with those recorded globally.

Relations between volcanic debris avalanche morphology and triggering mechanisms

The plan-view characteristics of the collapse scars and the avalanche deposits are included in the database. Although direct relationships have not yet been proven, the characterization of a scar's plan view morphology has been variably used to attempt to understand erosion processes, instability factors, and triggering mechanisms (e.g., Bernard et al. 2021). For example, horseshoe scars are mainly associated with eruption-related collapses, whereas triangular and large U-shaped scars are associated with deep-seated basement-related collapses affecting both volcanic edifice and underlying basement (e.g., Voight et al. 1981; van Wyk de Vries et al. 2001). The majority of events recorded in the database lack information on triggering mechanisms, although factors contributing to the destabilization of the volcano have been recognized in some cases.

Plan-view scars with a semicircular shape were identified in nine records (Figs. 5and 11; Supplementary material). This type of scar is observed in both large volcanic debris avalanches (area > 20 km²; e.g., Alto Quebrada Honda; Fig. 5d) and in several records of smaller ones (area < 5 km²; e.g., Quevar 1, 2, and 3; Fig. 5a). In the case of Llullaillaco's scar, it is likely that its original shape has been modified by subsequent activity. The collapse of Llullaillaco is linked to the extrusion of a dacitic flow, due to the presence of hot lava blocks in the proximal deposits and the steep slope of the residual structure (Richards and Villeneuve 2001). Regarding the

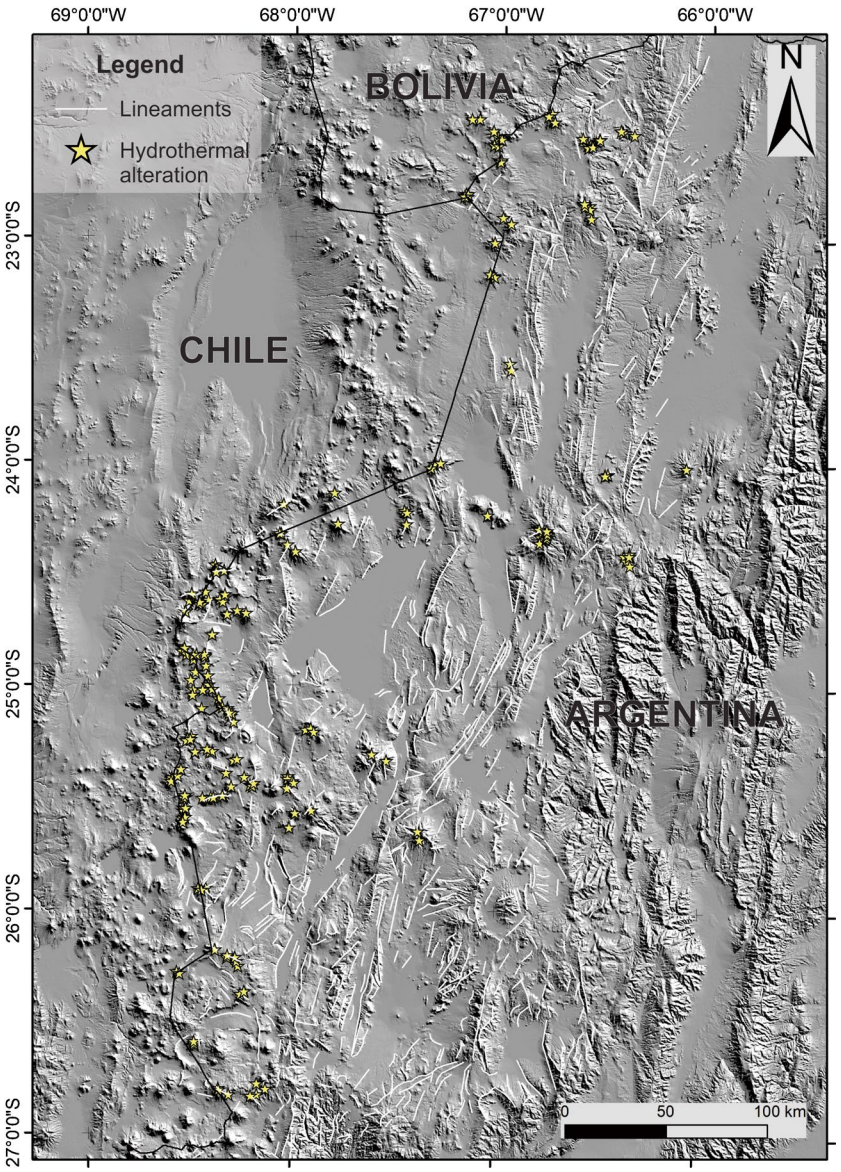

Fig. 9 Lineaments and hydrothermal alteration zones in NW Argentina. Background image is SRTM DEM-derived shaded relief

avalanche of the Negro de Chorrillos scoria cone, it is associated with gravitational instability resulting from its emplacement on a steeply inclined substrate (Urquizo 2012). All other records displaying semicircular scars have either been only mentioned by other authors or are identified for the first time in this work; hence, the collapse mechanisms cannot be definitively established.

Rectilinear scars were identified at the Chimpa and Tuzgle volcanoes. The unique collapse of the Chimpa volcano generated two parallel rectilinear scars (Fig. 4a), attributed to gravitational instability induced by tectonic faulting, hydrothermal alteration, and overloading (Norini et al. 2020). Tuzgle volcano also exhibits a rectilinear scar, likely originally a semicircular scar modified by post-collapse volcanic activity (Fig. 4b). The collapse of Tuzgle is linked to regional and local tectonics, intrusion direction, local slope, and a potential magmatic contribution (Norini et al. 2014). In both cases, the possible relation with a significant tectonic regime affecting the stability of the volcanoes generated rectilinear scars.

Three triangular-shaped scars were identified on the Socompa, Lastarria, and Cueros de Purulla volcanoes. In these cases, specific triggers are not recognized, but destabilizing factors differ. Several factors may have contributed to the destabilization of the Socompa edifice, including tectonic and seismic activity, progressive shear weakening, loading, magma intrusion, and explosive eruption (Francis et al. 1985; Francis and Self 1987; Ramírez 1988; Wadge et al. 1995; van Wyk de Vries et al. 2001). However, the trigger responsible for the largest collapse in the Central Andes, the Socompa collapse, remains unknown. Recently, Grosse et al. (2022) have suggested a potential relationship between the collapse and the last major glacial peak in the region, considering factors such as glacial unloading and permafrost loss. The trigger for the partial

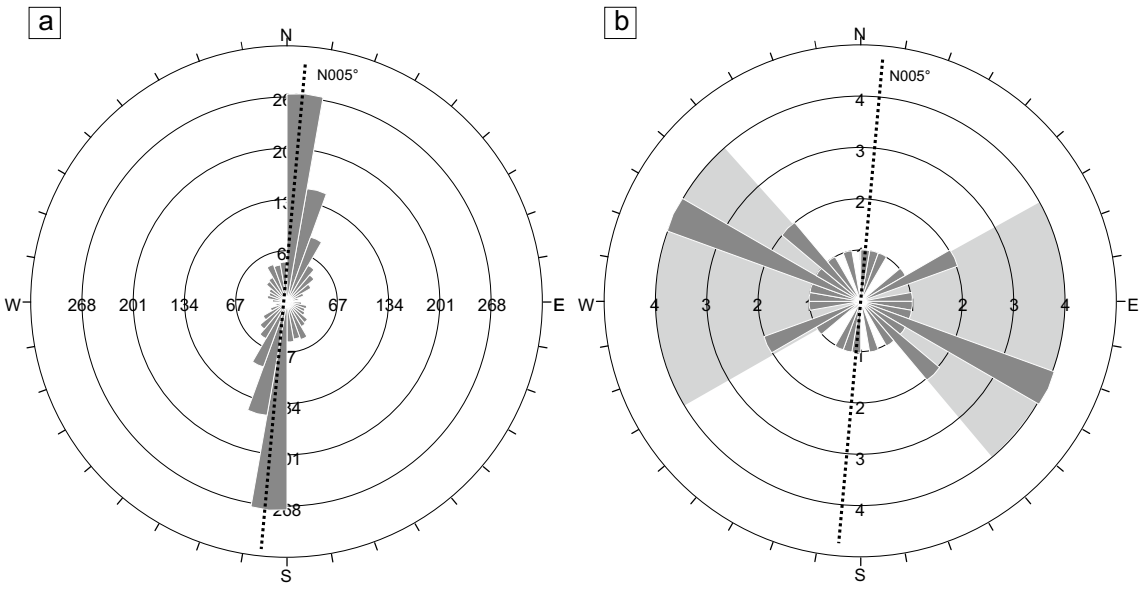

Fig. 10 **a** Rose diagram constructed from the lineaments identified in the studied area ($n = 1015$). The regional predominance is NNE–SSW (N 005°). **b** Rose diagram of the avalanche trajectories (scar azimuth or gamma angle). The more frequent directions are highlighted as shaded regions. The predominant regional trend of lineaments is shown as a dotted black-line

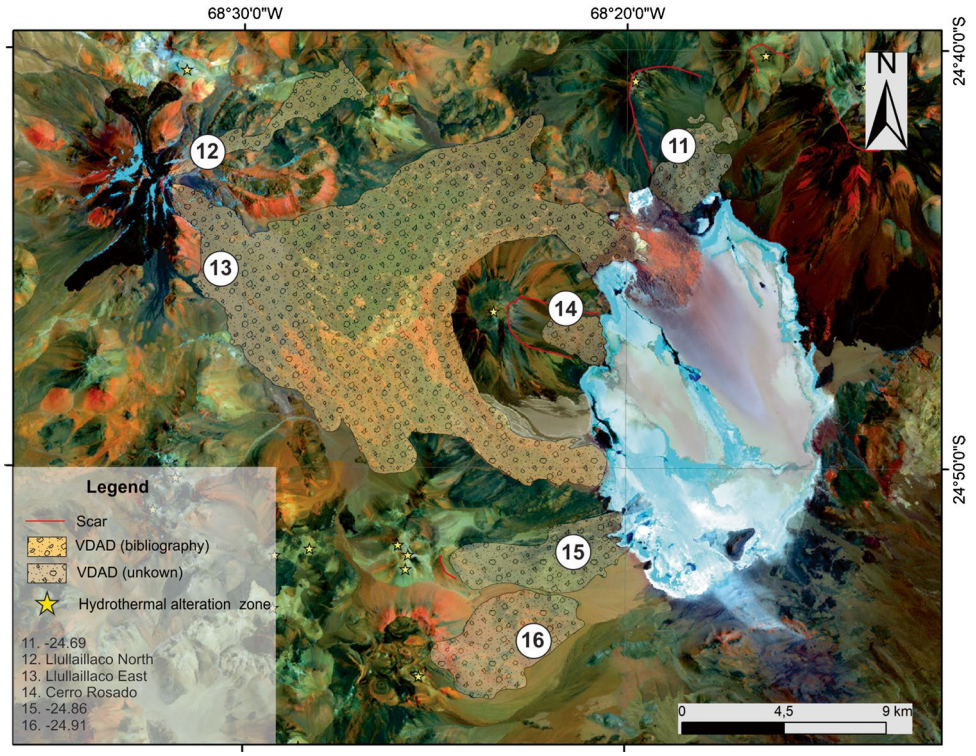

Fig. 11 Landsat 7 EMT + RGB 742 of the Llullaillaco area showing the relation between several VDAD with hydrothermal alteration zones

failure of the Lastarria volcano was proposed by Naranjo (2010) to be the result of rapid magma mixing between andesitic and low-temperature silica-rich magmas, potentially leading to eruptions that could activate a collapse. In contrast, Rodríguez et al. (2020) emphasize the association with the weakened core of the apparatus due to hydrothermal alteration (Rodriguez et al. 2020). The causes of the collapse of the Cueros de Purulla dome complex are not documented. Bertea et al. (2021) infer that gravitational destabilization

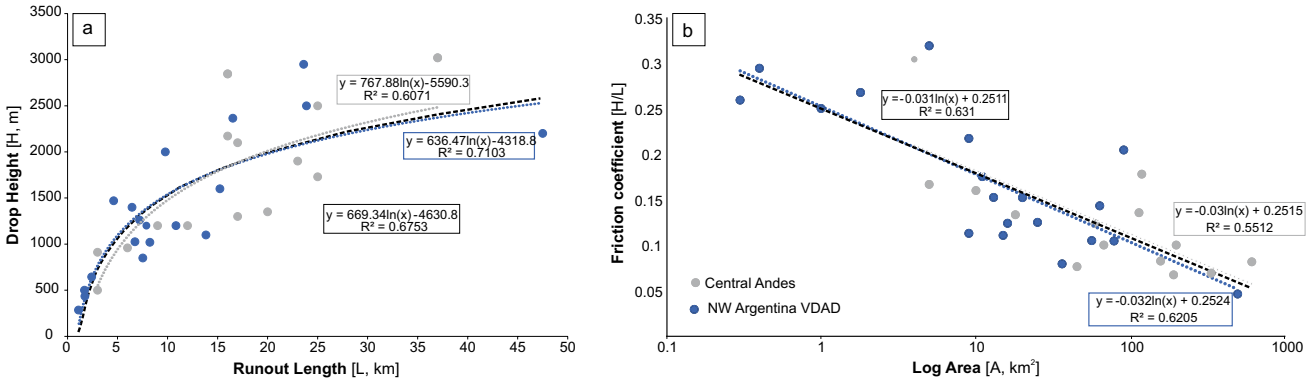

Fig. 12 Plots comparing geometric parameters of volcanic debris avalanche deposits. **a** Drop height vs runout length. **b** Log area vs friction coefficient. The gray dotted line represents the regression line of Central Andes volcanic avalanche deposits from Francis and Wells (1988). The blue dotted line represents the regression line of volcanic avalanche deposits from this work. The black dotted line represents the regression line of both datasets

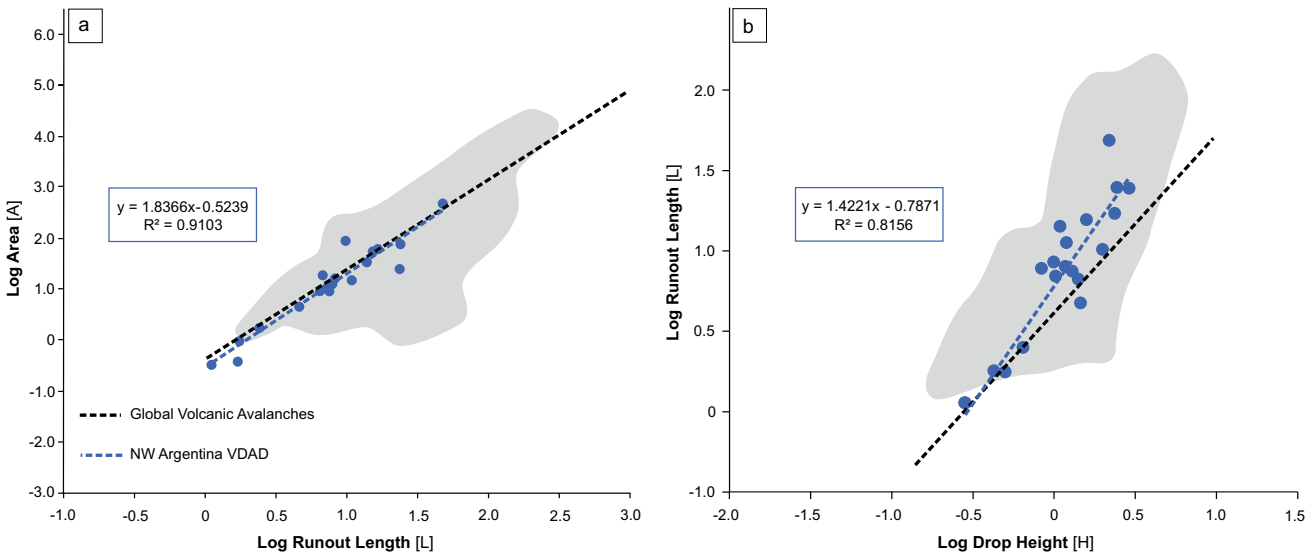

Fig. 13 Log–log plots comparing geometric parameters of volcanic debris avalanche deposits. **a** Area vs runout distance. **b** Drop height vs runout distance. The gray field represents the volcanic avalanche deposits from Dufresne et al. (2021b). The black dotted line represents the regression line of volcanic avalanche deposits from Dufresne et al. (2021b). The blue points represent the volcanic avalanche deposits from this work. The blue dotted line represents the regression line of volcanic avalanche deposits from this work

due to the rise of new magma in the conduit area, a seismic event, and the fact that the volcano is located on a steep slope may have been contributing factors. Given the aforementioned, it is not possible to correlate the plan-view shape of the scars with the triggering mechanism.

Rincón (Fig. 5b) and Cerro Rosado (Fig. 5c) present U-shaped scars. The deposits at Cerro Rosado are of small dimensions, occupying an area of less than 5 km², while Rincón exhibits a large collapse. Both examples lack detailed studies of the deposits, so it is not possible to establish whether basement involvement occurred in these collapses (e.g., Voight et al. 1981; van Wyk de Vries et al. 2001). However, considering the magnitude of the events, this could be possible only in the case of Rincón (Fig. 5b).

The scar outlined on the Aracar volcano has an irregular shape in the plan view (Fig. 5b). It is noteworthy that the deposit found at the base of this volcanic edifice might not correspond to this volcano. Detailed studies are needed to determine the lithologies included in the deposit to establish whether Aracar is the source of this collapse. Another possibility is that the collapse is related to the Pular event, as indicated by Zappettini et al. (2001).

The plan-view shapes of the volcanic debris avalanche deposits show variability. It has been hypothesized that there might be a connection between the pre-collapse topography and the morphology of the resulting deposit. Many deposits exhibit elongated shapes resulting from confinement within the topography (Fig. 11). Some deposits have a bifurcated distal zone, navigating topographic

obstacles, as observed in Lastarria and the eastern avalanche of Llullaillaco (Fig. 11). In contrast, there are avalanches with unrestricted mobility, forming a broad fan-shaped plan view as they are not confined by the topography (e.g., Tuzgle, Cueros de Purulla). Additionally, several examples exhibit indistinct shapes categorized here as irregular. In some cases, there is limited material mobility, with accumulation occurring at the base of the scar (e.g., Cerro Rosado and − 24.69 in Fig. 11).

Volcano collapse destabilizing factors in NW *Argentina*

It is often challenging to determine the triggers of volcanic debris avalanches, but the evaluation of the destabilizing factors contributing to the collapse of volcanic edifices is more feasible (e.g., Roverato et al. 2021; Siebert and Reid 2023). Faulting and hydrothermal alteration zones, together with steep slopes, magma intrusion, climatic fluctuations, increasing pore fluid pressures, and basement deformation, can all contribute to volcano destabilization. Therefore, we assessed the relationship between volcano collapses, regional tectonics, and hydrothermal alteration zones.

The morphology of volcanic edifices, collapse directions, and fracture planes are influenced by the regional stress fields (e.g., Zernack and Procter 2021). The orientation of volcanic avalanches may be controlled by the regional and local stress framework (e.g., Nakamura 1977; Lagmay et al. 2000). Generally, the prevalent direction of collapse is perpendicular to the maximum horizontal stress direction (Moriya 1980; Siebert 1984). It is important to highlight that volcanoes can generate their own local stress field and affect the regional stress framework due to gravitational loading (e.g. Marques and Cobbold 2002).

We found that lineaments in the study region have a dominant NNE–SSW trend orientation (Figs. 9 and 10), in agreement with Francis and Wells (1988) for the Central Andes. Most identified debris avalanche directions are perpendicular to this regional trend. However, not all of the studied deposits have this perpendicular direction to the regional structural trend. This is the case of several avalanche deposits located in the COT area, such as Tuzgle (avalanche directed towards the north), Rincón (SE), and Quevar 3 (SSW). These deviations can be explained by the fact that the destabilization direction of a volcano flank also depends on the position of faults within the volcanic edifice and the stress field (e.g., Wooller et al. 2009; Norini et al. 2020). The volcanic debris avalanche deposits in the COT area are situated within a tectonic framework characterized by horizontal compression with an E–W trending σ_1 (Norini et al. 2013). This configuration has been present since the Eocene–Oligocene. Since the Miocene, the COT has developed a sub-vertical transfer fault system that has evolved alongside N-S thrusts (Norini et al. 2013). Concurrent with the maximum horizontal stress and the COT fault system, hydrofractures develop in the volcanoes. In this context, local faults occur in volcanic systems, contributing to destabilization and thereby influencing the direction of collapse. This is the case for the Tuzgle volcano, where the volcanic debris avalanche deposits are dispersed to the north, perpendicular to the regional main principal stress.

Volcanoes often host hydrothermal alteration systems, leading to chemical modification of minerals, increasing clay content, and elevated pore pressure, which can persist over extended periods (e.g., van Wyk de Vries et al. 2001; Roverato et al. 2021). The hydrothermal alteration zones have the effect of weakening the volcanic edifice, reducing the strength of the rocks, and hence promoting its collapse. Breached volcanoes typically exhibit a hydrothermal alteration halo at their summits (e.g., Zernack 2021), and hydrothermal alteration has been identified as a contributing factor to collapse at Chimpa (Norini et al. 2020) and Lastarria volcanoes (Rodriguez et al. 2020). We have identified the presence of hydrothermal alteration zones at half of the avalanche records, which implies that hydrothermal alteration may be an important destabilizing factor in NW Argentina.

The surficial processes that regulate volcanic avalanches are mainly controlled by climate, which is more straightforward to identify in modern volcanic edifices than in older ones (e.g., Roberti et al. 2021). For example, edifice failures have been shown to be more common during humid periods and deglaciation due to glacial debuttressing, load discharge, and fluid circulation, particularly at the end of glaciations (e.g., Capra 2006; Morino et al. 2019; Roberti et al. 2021). In NW Argentina, glaciation was restricted to high-altitude glaciers and manifested in cyclical periods of humidity and aridity (e.g., Igarzábal 1984; Godfrey et al. 2003; López Steinmetz and Galli 2015; Zech et al. 2017; D'Arcy et al. 2019). In this regard, considering the observations made by Grosse et al. (2022), it is noted that the volcanic debris avalanches at Socompa (6.18 ka; Grosse et al. 2022) and Lastarria (7.5 ka, Rodríguez et al. 2020) occurred thousands of years following the glacial retreat of the last main glacial peak in the area, which ended ~ 10 to 12 ka (e.g., Thompson et al. 1998; Martini et al. 2017) in the Central Andes. The connection of volcanic collapse to glacial unloading or permafrost loss is hence speculative as a triggering mechanism.

Uses of the database

The database presents standardized and consistent information on volcanic debris avalanches in NW Argentina. It compiles both published and unpublished data regarding scars and volcanic debris avalanche deposits in the region. This digital repository is accessible via the IBIGEO website to researchers and governmental authorities responsible for the geological risk assessment of the country (i.e., SEGEMAR in Argentina). Researchers can use the database to recognize gaps of knowledge, identify patterns, distinguish areas with high risk, etc. Our goal is to continuously update and expand the database by incorporating records from across the Central Volcanic Zone (CVZ) region and integrating newly published data. Additionally, we plan to include additional morphometric parameters and quantify morphological features in the future.

While an exhaustive search for distinctive features of scars and avalanche deposits was conducted using digital elevation models, it is important to acknowledge that this database is inevitably incomplete and may contain errors. Some features may be obscured due to the deposition of new material or erosion of volcanic structures, or they may not be discernible at the spatial resolution of the DEMs used. Therefore, it is crucial to supplement and validate this database through detailed fieldwork in the future.

Conclusions

Nineteen collapse records are cataloged in the new remote-sensing-based volcanic debris avalanche database of Northwest Argentina. Morphometric parameters, derived from the 12-m spatial resolution

TanDEM-X DEMs, of the scar and volcanic debris avalanche deposits characterize each of these collapse events. This study has identified eleven previously undocumented scars and their associated volcanic debris avalanche deposits. Fieldwork is essential for validating these presumed volcanic collapses.

Consistent with global trends, the majority of collapse events recorded in this database originate from composite volcanoes. Collapse directions occur mainly perpendicular to regional structures, indicating the strong influence of the tectonic framework. Instances where collapse directions deviate from this norm may be attributed to local-scale factors specific to each volcano. Notably, half of the collapse records indicate the presence of hydrothermal alteration areas at the volcano summits, suggesting that hydrothermal weakening is a significant destabilizing factor in the region.

The synthesis of information in this database constitutes a valuable tool for understanding the spatial relationships and temporal distribution of volcanic debris avalanches in the context of the Central Volcanic Zone of the Andes. The condensed information facilitates easy access and allows for comparisons between scar and deposit parameters. This enables the establishment of relationships with the source volcanic edifices and facilitates linkage to collapse-triggering features, such as hydrothermal alteration zones and tectonic structures. Moreover, the database illuminates research gaps, providing insights into which volcanic edifices and associated collapse deposits require further study or lack sufficient characterization.

Several records in this database are solely based on remote assessments. It is imperative to underscore the importance of field studies in confirming or refuting these findings.

Acknowledgements

We acknowledge Federico Di Traglia and one anonymous reviewer for their helpful and constructive comments. Also, we would like to thank Jan Blahut for kindly handling our paper.

Funding

This work was supported by the PIBAA 28720210100094CO and PICT-2021-GRFTI-00145 grants to Emilce Bustos.

Data Availability

I declare that the data supporting this study are available upon request from the corresponding author.

Declarations

Competing interests The authors declare no competing interests.

References

Aaron J, McDougall S (2019) Rock avalanche mobility: the role of path material. Eng Geol 257:105126

Acocella V, Gioncada A, Omarini R, Riller U, Mazzuoli R, Vezzoli L (2011) Tectonomagmatic characteristics of the back-arc portion of the Calama–Olacapato–El Toro Fault Zone, Central Andes. Tectonics 30(3):TC3005. https://doi.org/10.1029/2010TC002854

Allmendinger RW, Ramos VA, Jordan TE, Palma M, Isacks BL (1983) Paleogeography and Andean structural geometry Northwest Argentina. Tectonics 2(1):1–16

Auker MR, Sparks RSJ, Siebert L, Crosweller HS, Ewert J (2013) A statistical analysis of the global historical volcanic fatalities record. J Appl Volcanol 2(1):1–24

Báez W, Bustos E, Chiodi A, García HPA, Álvarez O, Simón V, Folguera A (2023) Reviewing the geodynamic impact of aseismic ridges subduction on the tectonic-magmatic evolution of the Southern Puna plateau. J S Am Earth Sci 129:104520

Bernard B, de Vries BVW, Barba D, Leyrit H, Robin C, Alcaraz S, Samaniego P (2008) The Chimborazo sector collapse and debris avalanche: deposit characteristics as evidence of emplacement mechanisms. J Volcanol Geoth Res 176(1):36–43

Bernard B, Takarada S, Andrade SD, Dufresne A (2021) Terminology and strategy to describe volcanic landslides and debris avalanches. In: Roverato M, Dufresne A, Procter J (eds) Volcanic debris avalanches: from collapse to hazard. Springer book series advances in volcanology 364

Bertea ES, Báez W, Bustos E, Filipovich R, Bardelli L, Arnosio M, Villagrán A, Sommer C, Alfaro B, Chiodi A (2021) Cartografía y reconstrucción de la historia eruptiva del volcán Cueros de Purulla, Puna Austral, Provincia de Catamarca. Revista de la Asociación Geológica Argentina 78(2):284–310

Blahůt J, Balek J, Klimeš J, Rowberry M, Kusák M, Kalina J (2019) A comprehensive global database of giant landslides on volcanic islands. Landslides 16(10):2045–2052

Blasco G, Zappettini EO, Hongn F (1996) San Antonio de los Cobres. Programa Nacional de Cartas Geológicas de la República Argentina 1:250.000. Hoja Geológica 2566-I. Provincias de Jujuy y de Salta. Boletín 217. Buenos Aires, Servicio Geológico Minero Argentino. Instituto de Geología y Recursos Minerales

Bustos E, Arnosio M, Báez W, Norini G, Suzaño NO, Viramonte JG (2020) Geomorphological evolution of the Chimpa stratovolcano in the back-arc region of the Central Andes. Geomorphology 364:107251

Bustos E, Capra L, Arnosio M, Norini G (2022) Volcanic debris avalanche transport and emplacement at Chimpa volcano (Central Puna, Argentina): insights from morphology, grain-size and clast surficial textures. J Volcanol Geoth Res 432:107671

Capra L (2006) Abrupt climatic changes as triggering mechanisms of massive volcanic collapses. J Volcanol Geoth Res 155(3–4):329–333

Capra L, Macías JL, Scott KM, Abrams M, Garduño Monroy VH (2002) Debris avalanches and debris flows transformed from collapses in the Trans-Mexican Volcanic Belt, Mexico—behavior, and implications for hazard assessment. J Volcanol Geoth Res 113:81–110. https://doi.org/10.1016/S0377-0273(01)00252-9

Clavero J, Sparks R, Huppert H, Dade W (2002) Geological constraints on the emplacement mechanism of the Parinacota debris avalanche, northern Chile. Bull Volcanol 64(1):40–54

Coira B, Caffe P, Ramírez A, Chayle W, Díaz A, Rosas S, Pérez A, Pérez B, Orozco O, Martínez YM (2004) Hoja Geológica 2366-I / 2166-III, Mina Pirquitas. Provincia de Jujuy. Instituto de Geología y Recursos Minerales, Servicio Geológico Minero Argentino, Buenos Aires. Boletín 269:122

D'Arcy M, Schildgen TF, Strecker MR, Wittmann H, Duesing W, Mey J, Tofelde S, Weissmann P, Alonso RN (2019) Timing of past glaciation at the Sierra de Aconquija, northwestern Argentina, and throughout the Central Andes. Quat Sci Rev 204:37–57. https://doi.org/10.1016/j.quascirev.2018.11.022

Davies T, McSaveney M, Kelfoun K (2010) Runout of the Socompa volcanic debris avalanche, Chile: a mechanical explanation for low basal shear resistance. Bull Volcanol 72:933–944

de Silva SL (1989) Altiplano-Puna volcanic complex of the central Andes. Geology 17(12):1102–1106

Devoli G, De Blasio FV, Elverhøi A, Høeg K (2009) Statistical analysis of landslide events in Central America and their run-out distance. Geotech Geol Eng 27:23–42

Dufresne A, Siebert L, Bernard B, Sparks RSJ, Takarada S, Clavero J, Belousov A, Belousova M (2008) Volcanic debris avalanche deposit database—a progress report. Abstr, IAVCEI general assembly, Reykjavík, Iceland August 17–22, 2008

Dufresne A, Zernack A, Bernard K, Thouret JC, Roverato M (2021a) Sedimentology of volcanic debris avalanche deposits. In: Roverato M, Dufresne A, Procter J (eds) Volcanic debris avalanches,

Springer, Cham. Adv Volcanol 6:175–210. https://doi.org/10.1007/978-3-030-57411-6_8
Dufresne A, Siebert L, Bernard B (2021b) Distribution and geometric parameters of volcanic debris avalanche deposits In: Roverato M, Dufresne A, Procter J (eds) Volcanic debris avalanches, Springer, Cham. Adv Volcanol 6:75–90. https://doi.org/10.1007/978-3-030-57411-6_4
Elmasri R, Navathe SB (2011) Database systems, vol 9. Pearson Education, Boston, MA
Francis P, Self S (1987) Collapsing volcanoes. Sci Am 256(6):90–99
Francis PW, Wells GL (1988) Landsat Thematic Mapper observations of debris avalanche deposits in the Central Andes. Bull Volcanol 50(4):258–278
Francis PW, Gardeweg M, Ramirez CF, Rothery DA (1985) Catastrophic debris avalanche deposit of Socompa volcano, northern Chile. Geology 13(9):600–603
Giles JR (1995) The what, why, when, how, where and who of geological data management. Geological Society, London, Special Publications 97(1):1–4
Global Volcanism Program (2024) [Database] volcanoes of the world (v. 5.2.0; 6 Jun 2024). Distributed by Smithsonian Institution, compiled by Venzke, E. https://doi.org/10.5479/si.GVP.VOTW5-2024.5.2
Godfrey LV, Jordan TE, Lowenstein TK, Alonso RN (2003) Stable isotope constraints on the transport of water to the Andes between 22° and 26°S during the last glacial cycle. Palaeogeogr Palaeoclimatol Palaeoecol 194:299–316
Godoy BG, Clavero J, Rojas C, Godoy E (2012) Volcanic facies of the debris avalanche deposit of Tata Sabaya Volcano Central Andes. Andean Geol 39(3):394–406
Godoy B, Rodríguez I, Pizarro M, Rivera G (2017) Geomorphology, lithofacies, and block characteristics to determine the origin, and mobility, of a debris avalanche deposit at Apacheta-Aguilucho Volcanic Complex (AAVC), northern Chile. J Volcanol Geoth Res 347:136–148
Grosse P, van Wyk de Vries B, Petrinovic IA, Euillades PA, Alvarado GE (2009) Morphometry and evolution of arc volcanoes. Geology 37(7):651–654
Grosse P, Euillades PA, Euillades LD, Wyk V, de Vries B (2014) A global database of composite volcano morphometry. Bull Volcanol 76:1–16
Grosse P, Guzmán S, Petrinovic IA (2017) Volcanes compuestos cenozoicos del noroeste argentino. In: Muruaga CM, Grosse P (eds) Ciencias de la Tierra y Recursos Naturales del NOA 484–517 (Relatorio del XX Congreso Geológico Argentino)
Grosse P, Danišík M, Apaza FD, Guzmán SR, Lahitte P, Quidelleur X, Self S, Siebe C, van Wyk de Vries B, Ureta G, Guillong M, De Rosa R, Le Roux P, Wotzlaw J-F, Bachman O (2022) Holocene collapse of Socompa volcano and pre-and post-collapse growth rates constrained by multisystem geochronology. Bull Volcanol 84(9):1–18. https://doi.org/10.1007/s00445-022-01594-0
Hasan E, Fagin T, El Alfy Z, Hong Y (2016) Spectral Angle Mapper and aeromagnetic data integration for gold-associated alteration zone mapping: a case study for the Central Eastern Desert Egypt. Int J Remote Sens 37(8):1762–1776
Hongn D, Seggiaro RE, Monaldi CR, Alonso RN, González RE, Igarzábal AP, Ramallo E, Godeas M, Fuertes A, García R, Moya F, González O (2001) Hoja Geológica 2566-III, Cachi. Provincias de Salta y Catamarca. Instituto de Geología y Recursos Minerales, Servicio Geológico Minero Argentino, Buenos Aires. Boletín 248:94
Igarzabal A (1984) Origen y evoluci6n geomorfol6gica de las cuencas evaporiticas cuartarias de la Puna argentina. In: Actas, IX Congr Geol Argent 3:595–607
Inokuchi T (2006) Properties of sector-collapse and debris avalanche on Quaternary volcanoes in Japan. J Japan Landslide Soc 42(5):409–420
James DE (1971) Plate tectonic model for the evolution of the Central Andes. Geol Soc Am Bull 82(12):3325–3346
Jicha BR, Laabs BJ, Hora JM, Singer BS, Caffee MW (2015) Early Holocene collapse of Volcán Parinacota, Central Andes, Chile: volcanological and paleohydrological consequences. Bulletin 127(11–12):1681–1688
Kay SM, Coira BL (2009) Shallowing and steepening subduction zones, continental lithospheric loss, magmatism, and crustal flow under the Central Andean Altiplano-Plateau. In: Kay SM, Ramos VA, Dickinson WR (eds) Backbone of the Americas: plateau uplift, shallow subduction and ridge collision, vol 204. Geological Society of America Memoir, pp 229–259. https://doi.org/10.1130/2009.1204(11)
Kelfoun K, Druitt T, Wyk B, van deVries, Guilbaud MN (2008) Topographic reflection of the Socompa debris avalanche, Chile. Bull Volcanol 70:1169–1187
Kelfoun K, Druitt TH (2005) Numerical modeling of the emplacement of Socompa rock avalanche, Chile. J Geophys Res: Solid Earth 110(B12). https://doi.org/10.1029/2005JB003758
Krieger G, Moreira A, Fiedler H, Hajnsek I, Werner M, Younis M, Zink M (2007) TanDEM-X: a satellite formation for high-resolution SAR interferometry. IEEE Trans Geosci Remote Sens 45(11):3317–3341
Laake A (2011) Integration of satellite imagery, geology and geophysical data. Earth and environmental sciences. InTech 467–492. https://doi.org/10.5772/27613
Lagmay AMF, van Wyk DeVries B, Kerle N, Pyle DM (2000) Volcano instability induced by strike-slip faulting. Bull Volcanol 62:331–346. https://doi.org/10.1007/s004450000103
Lindsay JM, Schmitt AK, Trumbull RB, De Silva SL, Siebel W, Emmermann R (2001) Magmatic evolution of the La Pacana caldera system, Central Andes, Chile: compositional variation of two cogenetic, large-volume felsic ignimbrites. J Petrol 42(3):459–486
Lopez Steinmetz RL, Galli CI (2015) Basin development at the eastern border of the northern Puna and its relationship with the plateau evolution. J S Am Earth Sci 63:244–259
MacLeod N (1989) Sector-failure eruptions in Indonesia volcanoes. Geol Indonesia 12:563–601
Marques FO, Cobbold P (2002) Topography as a major factor in the development of arcuate thrust belts: insights from sandbox experiments. Tectonophysics 348:247–268
Martini MA, Kaplan MR, Strelin JA, Astini RA, Schaefer JM, Caffee MW, Schwartz R (2017) Late Pleistocene glacial fluctuations in Cordillera Oriental, subtropical Andes. Quatern Sci Rev 171:245–259
McGuire WJ (1996) Volcano instability: a review of contemporary themes. Geological Society, London, Special Publications 110(1):1–23. https://doi.org/10.1144/GSL.SP.1996.110.01.01
Morino C, Conway SJ, Sæmundsson Þ, Helgason JK, Hillier J, Butcher FE, Balme MR, Jordan C, Argles T (2019) Molards as an indicator of permafrost degradation and landslide processes. Earth Planet Sci lett 516:136–147. https://doi.org/10.1016/j.epsl.2019.03.040
Moriya I (1980) History of Akagi volcano. Bull Volcanol Soc Jpn 15:120–131
Nakamura K (1977) Volcanoes as possible indicators of tectonic stress orientation—principle and proposal. J Volcanol Geoth Res 2(1):1–16
Naranjo JA, Francis P (1987) High velocity debris avalanche at Lastarria volcano in the north Chilean Andes. Bull Volcanol 49:509–514. https://doi.org/10.1007/BF01245476
Naranjo JA (2010) Geología del Complejo Volcánico Lastarria, Región de Antofagasta. Servicio Nacional de Geología y Minería, Carta Geológica de Chile, Serie Geología Básica, No. 123, 1:25,000 scale, 1 sheet, p 33.
Neall VE (2002) Review of flank collapses at New Zealand volcanoes. Montagne Pelee 1902–2002 Explosive volcanism in subduction zones, St. Pierre, Martinique, 12–16 May 2002, Abstr p 71
Norini G, Cogliati S, Baez W, Arnosio M, Bustos E, Viramonte J, Groppelli G (2014) The geological and structural evolution of the Cerro Tuzgle Quaternary stratovolcano in the back-arc region of the Central Andes, Argentina. J Volcanol Geoth Res 285:214–228
Norini G, Bustos E, Arnosio M, Baez W, Zuluaga MC, Roverato M (2020) Unusual volcanic instability and sector collapse configuration at Chimpa volcano, central Andes. J Volcanol Geoth Res 393:106807
Norini G, Baez W, Becchio R, Viramonte J, Giordano G, Arnosio M, Pinton A, Groppelli G (2013) The Calama–Olacapato–El Toro fault system in the Puna Plateau, Central Andes: geodynamic implications and stratovolcanoes emplacement. Tectonophysics 608:1280–1297. https://doi.org/10.1016/j.tecto.2013.06.013
Palmer BA, Alloway BV, Neall VE (1991) Volcanic-debris-avalanche deposits in New Zealand — lithofacies organization in unconfined, wet-avalanche flows. In: Fisher RV, Smith GA (eds) Sedimentation in volcanic settings: society of economic paleontologists and mineralogists special publication, vol 45. Society of Economic Paleontologists

and Mineralogists, Tulsa, Ok, pp 89–98. https://doi.org/10.2110/pec.91.45.0089
Parada MA, López-Escobar L, Oliveros V, Fuentes F, Morata D, Calderón M, et al. (2007) "Andean magmatism," in The geology of Chile. Editors T. Moreno and W. Gibbons (London: The Geological Society), 115–146. https://doi.org/10.1144/GOCH.4
Ramirez CF (1988) The geology of Socompa volcano and its debris avalanche deposit, northern Chile. MSc dissertation, Open University, Milton Keynes, UK, pp 146
Reid ME, Sisson TW, Brien DL (2001) Volcano collapse promoted by hydrothermal alteration and edifice shape, Mount Rainier. Wash Geol 29(9):779–782
Richards JP, Villeneuve M (2001) The Llullaillaco volcano, Northwest Argentina: construction by Pleistocene volcanism and destruction by sector collapse. J Volcanol Geoth Res 105(1–2):77–105
Riller U, Petrinovic I, Ramelow J, Strecker M, Oncken O (2001) Late Cenozoic tectonism, collapse caldera and plateau formation in the Central Andes. Earth Planet Sci Lett 188(3–4):299–311
Roberti G, Roberts NJ, Lit C (2021) Climatic Influence on Volcanic Landslides. In: Roverato M, Dufresne A, Procter J (eds) Volcanic Debris Avalanches. Advances in Volcanology. Springer, Cham. https://doi.org/10.1007/978-3-030-57411-6_6
Rodríguez I, Páez J, de Vries MSVW, de Vries BVW, Godoy B (2020) Dynamics and physical parameters of the Lastarria debris avalanche, Central Andes. J Volcanol Geoth Res 402:106990
Roverato M, Di Traglia F, Procter J, Paguican EMR, Dufresne A (2021) Factors contributing to volcano lateral collapse. In: Roverato M, Dufresne A, Procter J (eds) Volcanic debris avalanches: from collapse to hazard. Springer book series advances in volcanology 364
Salfity J (1985) Lineamientos transversales al rumbo andino en el noroeste argentino. In: Actas 4° Congreso Geologico Chileno, 2, pp. 119–137. Antofagasta.
Seggiaro RE, Hongn FD, Castillo A, Pereyra F, Villegas D, Martínez L (2006) Hoja Geológica 2769-II, Paso San Francisco, Provincia de Catamarca. Instituto de Geología y Recursos Minerales, Servicio Geológico Minero Argentino, Buenos Aires. Boletín 294:62
Seggiaro R, Becchio R, Pereyra F, Martínez L (2007) Hoja Geológica 2569-IV, Antofalla, provincias de Catamarca y Salta. Instituto de Geología y Recursos Minerales. Servicio Geológico Minero Argentino, Buenos Aires. Boletín 343:62
Seggiaro RE, Becchio R, Bercheñi V, Ramallo L (2015) Hoja Geológica 2366-III Susques, provincias de Jujuy y Salta. Instituto de Geología y Recursos Minerales, Servicio Geológico Minero Argentino, Buenos Aires. Boletín 414:103
Shea T, van Wyk deVries B (2008) Structural analysis and analogue modeling of the kinematics and dynamics of rockslide avalanches. Geosphere 4:657–686
Siebert L (1984) Large volcanic debris avalanches: characteristics of source areas, deposits, and associated eruptions. J Volcanol Geoth Res 22(3–4):163–197
Siebert L, Reid ME (2023) Lateral edifice collapse and volcanic debris avalanches: a post-1980 Mount St Helens perspective. Bull Volcanol 85(11):61
Siebert L, Roverato M (2021) A historical perspective on lateral collapse and volcanic debris avalanches. In: Roverato M, Dufresne A, Procter J (eds) Volcanic debris avalanches. Advances in volcanology. Springer, Cham. https://doi.org/10.1007/978-3-030-57411-6_2
Siebert L, Kimberly P, Pullinger CR (2004) The voluminous Acajutla debris avalanche from Santa Ana volcano, western El Salvador, and comparison with other Central American edifice-failure events. In: Rose WI, Bommer JJ, López DL, Carr MJ, Major JJ (eds) Natural hazards in El Salvador: Boulder, Colorado, Geological Society of America Special Paper 375, p 5–23
Stern CR, Moreno H, López-Escobar L, Clavero JE, Lara LE, Naranjo JA, ... Skewes MA (2007) Chilean volcanoes. https://doi.org/10.1130/0-8137-2375-2.5
Thompson LG, Davis ME, Mosley-Thompson E, Sowers TA, Henderson KA, Zagorodnov VS, Lin PN, Mikhalenko VN, Campen RK, Bolzan JF, Cole-Dai J, Francou B (1998) A 25,000-year tropical climate history from Bolivian ice cores. Science 282:1858–1864
Thouret JC (1999) Volcanic geomorphology—an overview. Earth Sci Rev 47(1–2):95–131
Trumbull RB, Riller U, Oncken O, Scheuber E, Munier K, Hongn F (2006) The time-space distribution of Cenozoic volcanism in the south-central Andes: a new data compilation and some tectonic implications. In: Oncken O, Chong G, Franz G, Giese P, Gotze HJ, Ramos VA, Strecker MR, Wigger P (eds) The andes: active subduction orogeny. Springer-Verlag, Berlin, pp 29–43. https://doi.org/10.1007/978-3-540-48684-8_2
Turner P, Piovarci M, Tragheim D, Bateson L, Chacksfield B (2008) From paper maps to a new geoscience digital store: cartographic developments in the Precambrian geology of central and northern Madagascar. pp 309–311
Ui T, Yamamoto H, Suzuki-Kamata K (1986) Characterization of debris avalanche deposits in Japan. J Volcanol Geoth Res 29(1–4):231–243
Urquizo P (2012) Mecanismos de erupción y modelo de facies del volcán monogenético Negro de Chorrillos, Puna Salteña. Undergraduate Thesis. Salta University
van Wyk deVries B, Self S, Francis PW, Keszthelyi L (2001) A gravitational spreading origin for the Socompa debris avalanche. Journal of Volcanology and Geothermal Research 105(3):225–247. https://doi.org/10.1016/S0377-0273(00)00252-3
Viramonte JG, Galliski MA, Arana Saavedra V, Aparício A, García Cucho L, Martín Escorza C (1984) El finivulcanismo basico de la depresion de Arizaro, provincia de Salta. In: Actas 9° Congreso Geologico Argentino, 3, pp. 234–251. Bariloche
Voight B, Glicken H, Janda RJ, Douglass M (1981) Catastrophic rockslide avalanche of May 18 (Mount St. Helens). In: Lipman PW, Mulineaux DR (eds) The 1980 eruptions of Mount St. Helens, Washington. US geological survey professional paper, vol 12, pp 347–377
Wadge G, Francis PW, Ramirez CF (1995) The Socompa collapse and avalanche event. J Volcanol Geoth Res 66(1–4):309–336
Williams R, Rowley P, Garthwaite MC (2019) Reconstructing the Anak Krakatau flank collapse that caused the December 2018 Indonesian tsunami. Geology 47(10):973–976
Wooller L, van Wyk deVries B, Murray JB, Rymer H, Meyer S (2004) Volcano spreading controlled by dipping substrata. Geology 32(7):573–5766
Wooller L, van Wyk deVries B, Cecchi E, Rymer H (2009) Analogue models of the effect of long-term basement fault movement on volcanic edifices. Bull Volcanol 71:1111–1131
Zappettini EO, Blasco G, Ramallo EE, González OE (2001) Hoja geológica 2569-II Socompa. Provincia de Salta. Instituto de Geología y Recursos Minerales, Servicio Geológico Minero Argentino. Boletín 260, 62 p. Buenos Aires.
Zech J, Terrizzano CM, García Morabito E, Veit H, Zech R (2017) Timing and extent of late Pleistocene glaciation in the arid Central Andes of Argentina and Chile (22°-41°S). Geogr Res Lett 43:697–718. https://doi.org/10.18172/cig.3235
Zernack AV, Procter JN (2021) Cyclic growth and destruction of volcanoes. In: Roverato M, Dufresne A, Procter J (eds) Volcanic debris avalanches. Advances in Volcanology. Springer, Cham. https://doi.org/10.1007/978-3-030-57411-6_12
Zernack AV (2021) Volcanic debris-avalanche deposits in the context of volcaniclastic ring plain successions—a case study from Mt. Taranaki. In: Roverato M, Dufresne A, Procter J (eds) Volcanic debris avalanches. Advances in volcanology. Springer, Cham. https://doi.org/10.1007/978-3-030-57411-6_9

Supplementary Information The online version contains supplementary material available at https://doi.org/10.1007/s10346-024-02365-y.

Emilce Bustos (✉) · Walter Ariel Báez · Marcelo Arnosio
Instituto de Bio y Geociencias del NOA (IBIGEO, UNSa-CONICET), Av. 9 de Julio 14, A4405BBA Salta, Argentina

Emilce Bustos
Email: emilcebustos@gmail.com

Gianluca Norini
Istituto Di Geologia Ambientale E Geoingegneria, Consiglio Nazionale Delle Ricerche, Area Della Ricerca CNR - ARM3, Via Roberto Cozzi 53, 20125 Milan, Italy

Pablo Grosse
Consejo Nacional de Investigaciones Científicas y Técnicas (CONICET), Buenos Aires, Argentina

Pablo Grosse
Fundación Miguel Lillo, Miguel Lillo 251, 4000 San Miguel de Tucumán, Argentina

Lucia Capra
Instituto de Geociencias, Campus Juriquilla, Universidad Nacional Autónoma de México, Blvd. Juriquilla 3001, 76230 Juriquilla, Querétaro, México